THE ASTROPHYSICAL JOURNAL, 434:162–183, 1994 October 10

THE ASSOCIATION OF HIGH-LATITUDE MOLECULAR CLOUDS WITH H I GAS

BE-YOUNG GIR AND LEO BLITZ
Department of Astronomy, University of Maryland, College Park, MD 20742
AND
LORIS MAGNANI
Department of Physics and Astronomy, University of Georgia, Athens, GA 30602
Received 1991 August 12; accepted 1994 March 25

ABSTRACT

The relationship between the high Galactic latitude molecular clouds (HLCs) and associated atomic hydrogen gas is investigated. In a global study, we examined a total of 75 HLCs observed in the CO ($J = 1$–0) transition and found that all the HLCs are associated with H I gas in both position and velocity with most of the HLCs located along filamentary or looplike H I structures. A small-scale comparison, using Green Bank 43 m H I data toward 10 regions associated with 18 HLCs, shows that the positions of the CO and H I peaks are typically offset from one another by $\sim 1^\circ.5$, comparable to the linear size of the HLCs. No obvious pattern for these CO–H I offsets was found either in relation to the Galactic plane or to an arbitrary explosion center. Typical velocity dispersions of the CO and its associated H I are found to be 0.6 and 3.0 km s^{-1}, with a mean H I/CO linewidths ratio of 5.7, which is close to the square root of the ratio of mass of CO/H I possibly indicating energy equipartition between the two phases. The data suggest that the molecular clouds condensed from the atomic gas in situ, rather than having been entrained in the H I. Moreover, the data are consistent with formation from the H I by means of a phase transition in pressure equilibrium. A few cloud complexes are anomalous, perhaps indicating variants in how the clouds formed. We find a minimum total hydrogen column density of 5×10^{20} cm^{-2} and a minimum relative abundance of H_2 nucleons of 50% in the 18 clouds we observed. Two of the 10 observed H I clouds, those associated with the molecular clouds MBM 27–29 and MBM 53–55, show clear arclike structures and the latter appear to be expanding with a velocity of about 18 km s^{-1}. The kinetic energy of this expanding shell is estimated to be about 4×10^{49} ergs, consistent with having been produced as a result of a supernova explosion or a stellar wind.

Subject headings: ISM: clouds — ISM: molecules — radio lines: ISM

1. INTRODUCTION

At high Galactic latitudes (defined for the purposes of this paper to be $|b| > 25^\circ$) and within a few hundered pc of the Sun, dozens of low-mass ($M < 10^3\ M_\odot$), small ($d < 10$ pc) molecular clouds have been found and are known collectively as the high-latitude molecular clouds (hereafter referred to as HLCs). Their general properties were first described by Blitz, Magnani, & Mundy (1984) and Magnani, Blitz, & Mundy (1985, hereafter MBM). Although several of the HLCs are Lynds (1962) dark clouds, the majority of objects are translucent molecular clouds with visual extinctions $1 < A_v < 5$ mag (van Dishoeck & Black 1988). Most of the translucent HLCs are not bound by gravity (MBM; Keto & Myers 1986, hereafter KM); however, the clumps within them may be bound by the mean turbulent pressure of the interstellar medium (ISM) (Blitz 1991; Turner, Xu, & Rickard 1992). In regions of shock compression, when the pressure of the ISM is even larger than normal, conditions may be ripe for converting some of the atomic gas into molecular form. Thus, the presence of HLCs in shock-compressed regions may provide a clue to the formation and origin of these objects and, perhaps, molecular clouds in general.

The suggestion that HLCs formed in regions of the ISM compressed by shocks was originally invoked (e.g., Magnani 1987; Elmegreen 1988; Mebold, Heithausen, & de Vries 1988) before it was widely accepted that the thermal pressure of the ISM is a small fraction of the turbulent pressure (Spitzer 1978; Bloemen 1987). The need for shocks arose because the HLCs, which are in general not gravitationally bound, have an internal pressure higher than the thermal pressure of the ISM. However, we now know that the internal cloud pressures, which are themselves turbulent, are about equal to the turbulent pressure of the ISM (Blitz 1991). Furthermore, there is good morphological evidence that at least some of the HLCs formed in shocks (e.g., the map of clouds MBM 53–55; Blitz 1987). The shocks could, in principle, have been generated by supernova explosions or by stellar winds which can produce H I shells with relatively large pressures within them (e.g., Heiles 1979, 1984; Meyerdierks, Heithausen, & Reif 1991). Elmegreen (1988) suggested that the HLCs have condensed out of shock-compressed H I based on global LSR velocity and internal velocity dispersion considerations. If the HLCs have condensed out of shock-compressed gas in H I shells, then some of these shells should be relatively nearby and closely associated with the molecular clouds. This case was made for several HLCs in Ursa major by Meyerdierks et al. (1991), and a recent paper by Burrows et al. (1993) shows exactly this relationship between an H I shell in Eridanus and the high-latitude clouds MBM 18 and MBM 20.

In this paper we examine the association between HLCs and local H I gas on both global and local scales and examine the evidence that the molecular clouds formed recently from ambient H I, rather than being preexisting molecular gas entrained by expanding H I shells. Section 2 describes the observations and data reduction used for this study, while § 3 presents the results from both the large- and small-scale

analysis. The arguments for the association between H I and HLCs are discussed in § 4. In the final section, we summarize the results of the paper.

2. DATA AND OBSERVATIONS

2.1. CO ($J = 1$–0) *Data*

A total of 75 high-latitude molecular clouds from two different surveys are examined in this study. Fifty-seven of them, in the northern hemisphere, are from the MBM catalog; the remainder are from the KM southern survey. MBM observed and mapped many of these clouds in the CO ($J = 1$–0) transition line using the 5 m telescope at the Millimeter Wave Observatory near Fort Davis, Texas. The beamwidth is 2.'3 and the velocity resolution is typically 0.65 km s^{-1}. The maps were sampled every 10′ or 20′ and are thus considerably undersampled. Further details on the observations are presented in MBM. The KM observations were carried out with the Columbia University 1.2 m antenna at Cerro Tololo, Chile, with a HPBW of 8.'7 and a velocity resolution of 0.26 km s^{-1}, and are generally sampled every beamwidth. Other details on this survey can be found in KM.

2.2. H I *Data*

Two types of H I data are used in this study. For the large-scale study, a photographic representation of the H I emission at 21 cm from the observations of Heiles & Habing (1974) and Colomb, Pöppel, & Heiles (1980, hereafter CPH) is used. The data cover the whole range in l, and extend from $|b| = 10°$ to $|b| = 65°$, with velocities between -38 km s^{-1} and $+38$ km s^{-1}. The angular and velocity resolutions of these observations are 30′ and 2 km s^{-1} respectively, but the channel maps as presented in CPH are separated by 4 km s^{-1}. The maps are sampled every one-half beamwidth in Galactic longitude and every beamwidth in Galactic latitude.

For the small-scale study, we observed 21 cm emission toward 10 regions which contain a total of 18 MBM clouds. The areas observed in H I were chosen to be about 3 times larger in angular size than the CO-defined area of the MBM clouds. The observations were carried out with the NRAO[1] 43 m telescope at Green Bank, West Virginia in 1985. The front-end consisted of a receiver with dual cooled FET amplifiers and a hybrid mode feed that produced simultaneous linear polarizations. At the zenith, the total system temperature was typically bout 23–25 K and the main beam efficiency, η_B, was ~0.8 (F. J. Lockman, private communication). The spectometer was split into two receivers of 512 channels each, resulting in a bandwidth which covered ± 132 km s^{-1} centered at zero velocity with respect to the local standard of rest (V_{LSR}). The angular and velocity resolutions were 21′ and 0.52 km s^{-1}, respectively. The data were obtained in the frequency-switched mode, with the reference switched by an amount to the bandwidth. Sampling was accomplished at 10′ or 20′ intervals depending on the size of the molecular cloud. The integration time was 15 s and the rms noise in a typical spectrum ranges from 0.2–0.3 K. A parabolic baseline was removed from each spectrum using the technique outlined in Appendix B of Lockman, Jahoda, & McCammon (1986). Table 1 lists the central position, the size, and the sampling interval for each mapped region.

[1] The National Radio Astronomy Observatory is operated by Associated Universities, Inc., under contract with the National Science Foundation.

TABLE 1

H I OBSERVATIONS

Clouds (MBM)	Mapped Center R.A. (1950)	Mapped Center Decl. (1950)	Mapped Size ΔR.A.	Mapped Size ΔDecl.	Sampling
16	3^{h}19^m.0	12°00.'0	4.°5	4.°5	20′
18	3 54.0	2 00.0	3.0	3.0	10
20	4 33.0	−14 00.0	3.0	3.0	20
23–24	7 33.5	46 30.0	2.0	2.0	10
25	8 02.0	46 00.0	1.5	1.5	10
27–29	9 17.8	72 20.0	12.5	2.5	20
40	16 08.0	22 00.0	1.5	1.5	10
41–44	16 50.7	61 50.0	3.5	2.5	10
49	21 29.4	12 25.0	1.5	1.5	10
53–55	22 54.0	21 00.0	4.0	12.0	20

3. DATA ANALYSIS AND RESULTS

3.1. *Large-Scale Comparison of HLCs and* H I

To check how well the HLCs are associated with H I gas on a global scale, the positions of the HLCs are superposed on the CPH photos that encompass the mean radial velocity of the molecular clouds (Fig. 1 [Pl. 2–6]). The maps of Figure 1 are in Galactic coordinates; every 10° of longitude (l) and latitude (b) is indicated by a tick mark. The central velocity of each H I map is indicated next to that figure. It is clear from these maps that *all* of the HLCs (except one KM cloud, for which $b = -66.°3$, out of the range of CPH) are positionally associated with H I gas at the same velocity. In most cases, the H I gas is in filamentary or looplike structures. For instance, in Figure 1*e*, the $V = -4$ km s^{-1} panel, a large loop in the region of $l = 270°$ to $l = 30°$ and $b = -20°$ to $b = 50°$ can be easily identified. This loop is part of an expanding shell formed by stellar winds and supernove explosions of stars in Scorpio-Centaurus (Cappa de Nicolau & Pöppel 1986; de Geus 1988). Another example of an H I looplike structure appears in the same figure in the region of $l = 80°$ to $l = 95°$ and $b = -25°$ to $b = -45°$, with which the CO clouds MBM 53–55 are associated. This particular H I structure is found to be expanding (see § 3.5).

It is apparent from Figure 1 that these H I features are generally much larger in area than the molecular HLCs. In many cases, the molecular clouds are only minor constituents of the total gas content of a particular morphological feature. The association of the molecular clouds with the large-scale looplike H I features suggests that at least some of the HLCs have been affected by incident shocks. That is, looplike features imply explosions or outflows which in turn suggest the prior existence of shocks. To investigate whether the clouds have been formed from the H I, or are simply preexisting clouds entrained within an expanding H I feature, we examine the relationship between the H I and CO in greater detail below.

3.2. *Small-Scale Comparison of HLCs and* H I

3.2.1. H I *Spectral Analysis and Resulting Contour Maps*

The Green Bank H I data show that the strength and the complexity of the H I spectral lines vary considerably from cloud to cloud. This is clearly seen in Figure 2, a composite of H I spectra at the positions of the CO peak of each cloud. It is evident from the figure that in most cases, even where there are multiple H I components, there is one that is clearly associated with CO. Nevertheless, many of the clouds do not exhibit

1994ApJ...434..162G

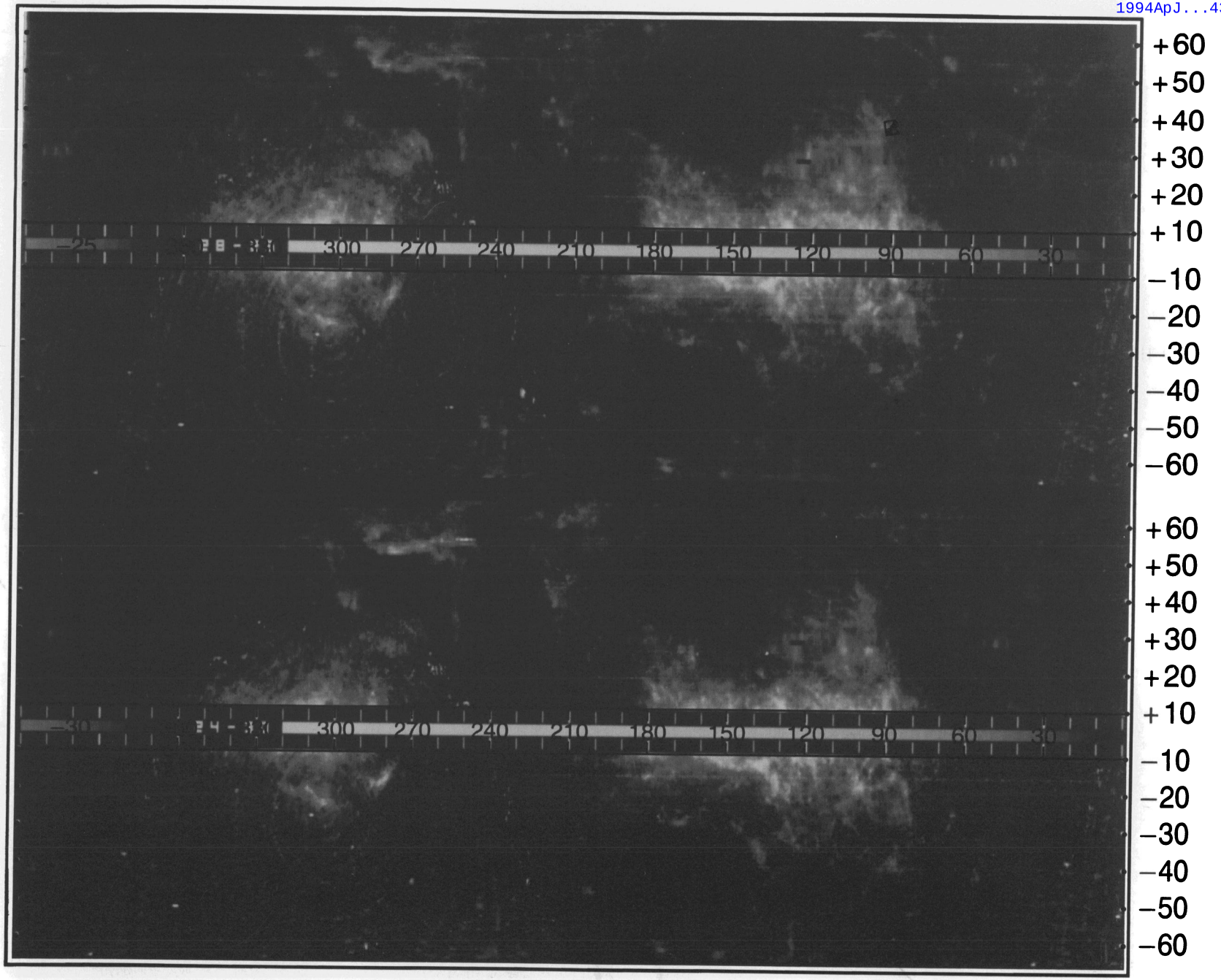

FIG. 1.—The HLCs superposed on the photographic representation of the H I data from Colomb, Pöppel, & Heiles (1980). The H I photos cover a latitude extent from $|b| = 10°$ to $|b| = 65°$ at all l, with tick marks to note every 10°. The velocity width of the H I in each panel is 4 km s^{-1}. The center velocity of each photo is marked next to it. The HLCs were plotted at their mean V_{LSR} on the H I photos at same velocity with dark dots.

1994ApJ...434..162G

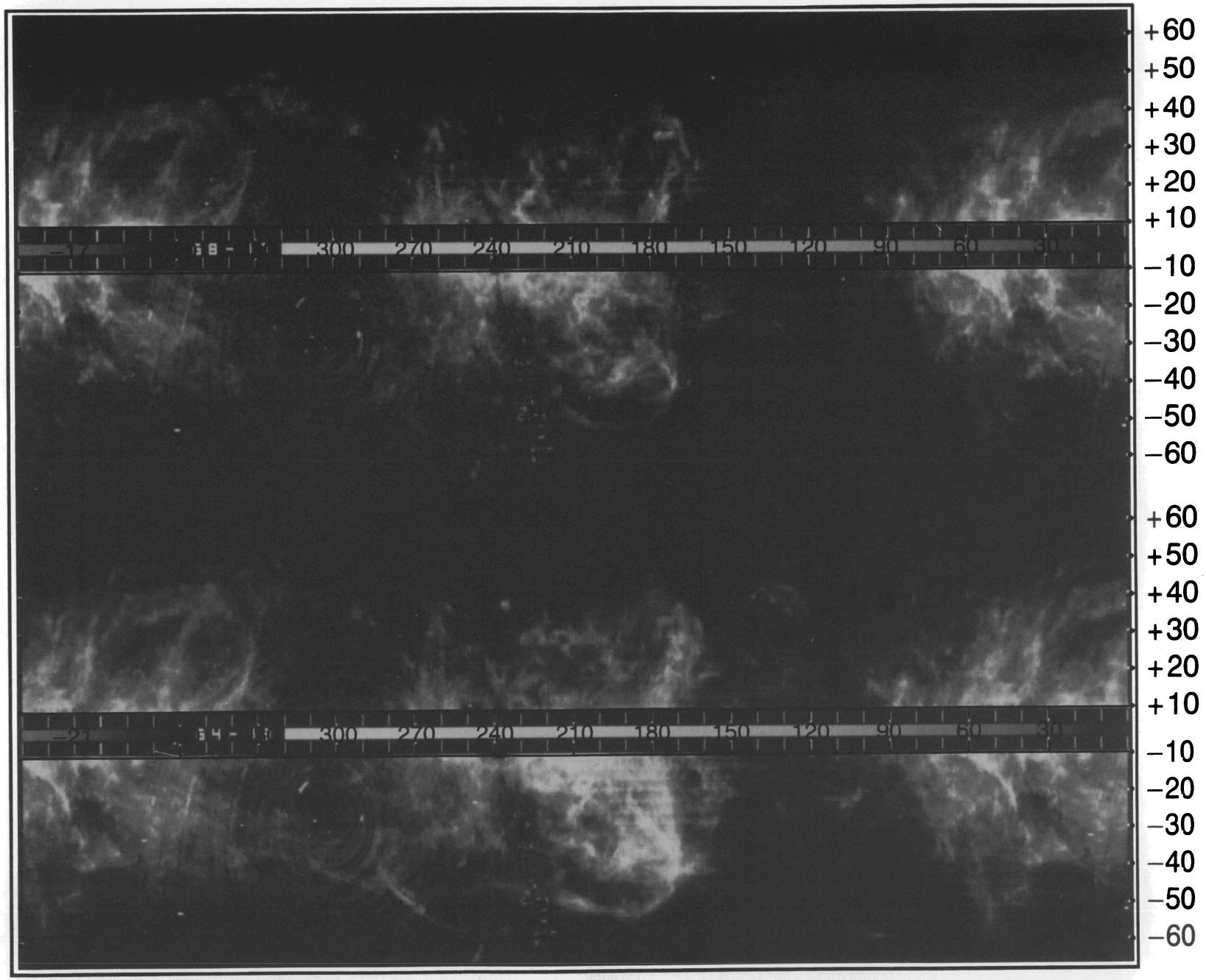

FIG. 1*b*

GIR, BLITZ, & MAGNANI (see 434, 163)

PLATE 3

PLATE 4

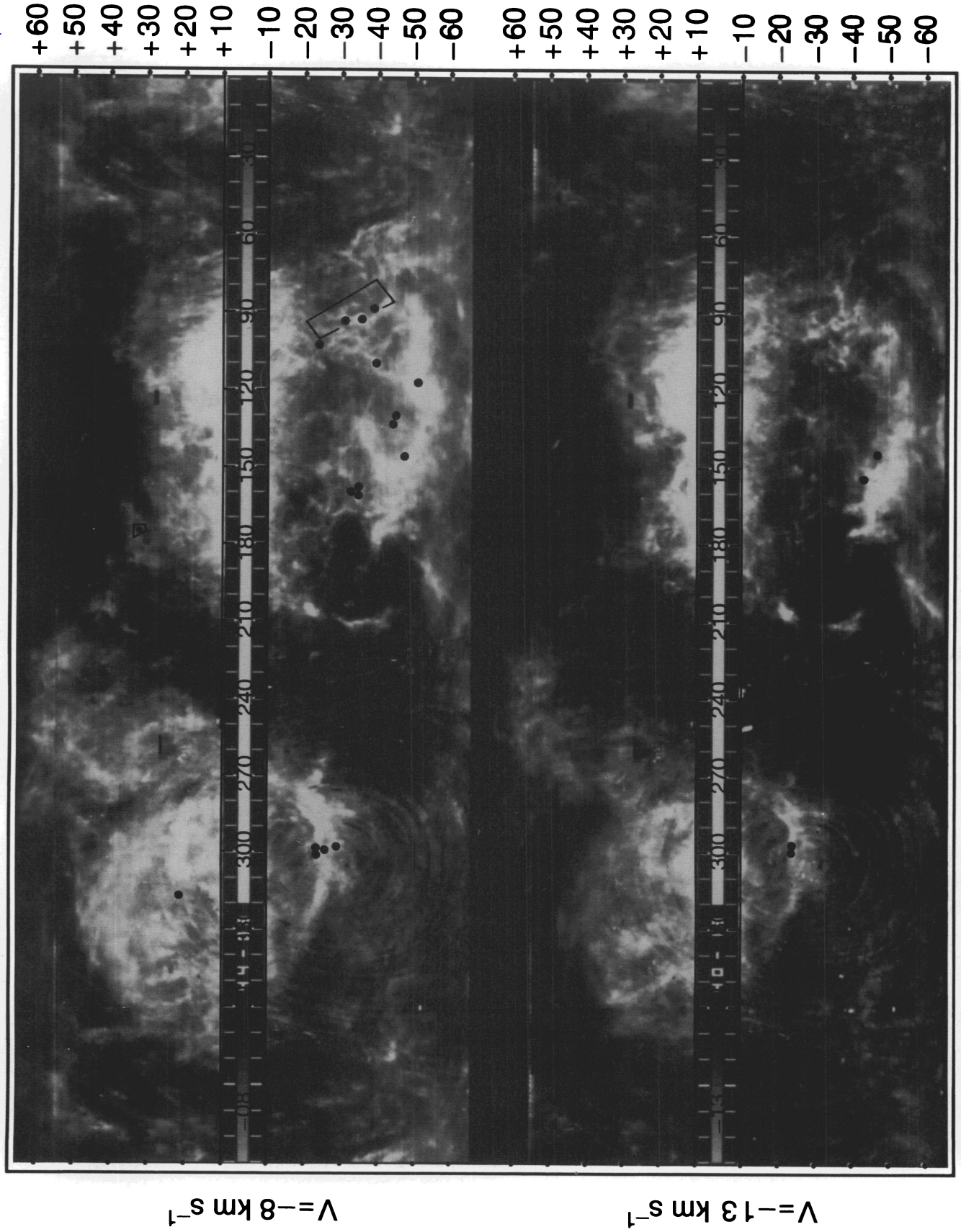

FIG. 1c

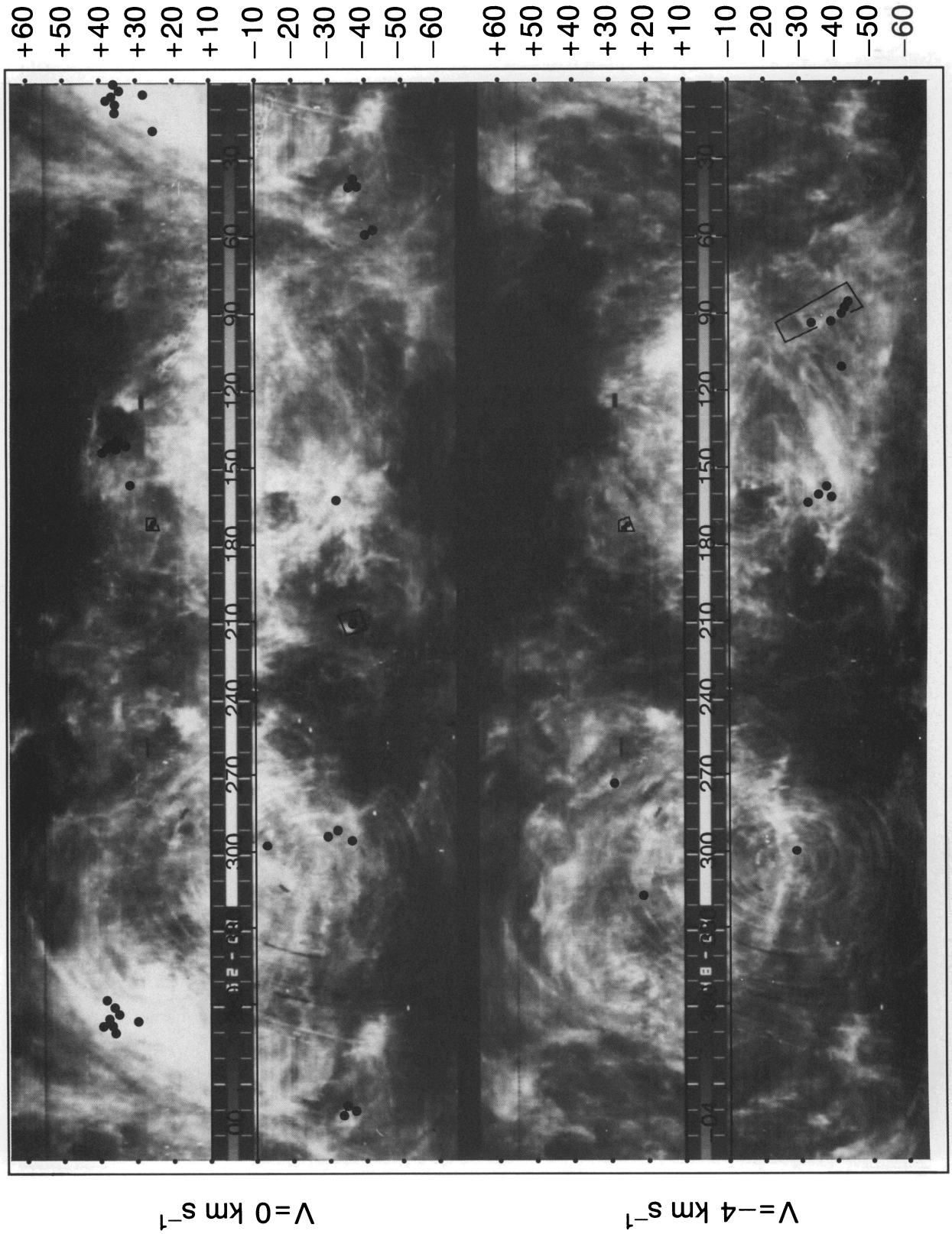

FIG. 1*d*

GIR, BLITZ, & MAGNANI (see 434, 163)

PLATE 6

FIG. 1e

GIR, BLITZ, & MAGNANI (see 434, 163)

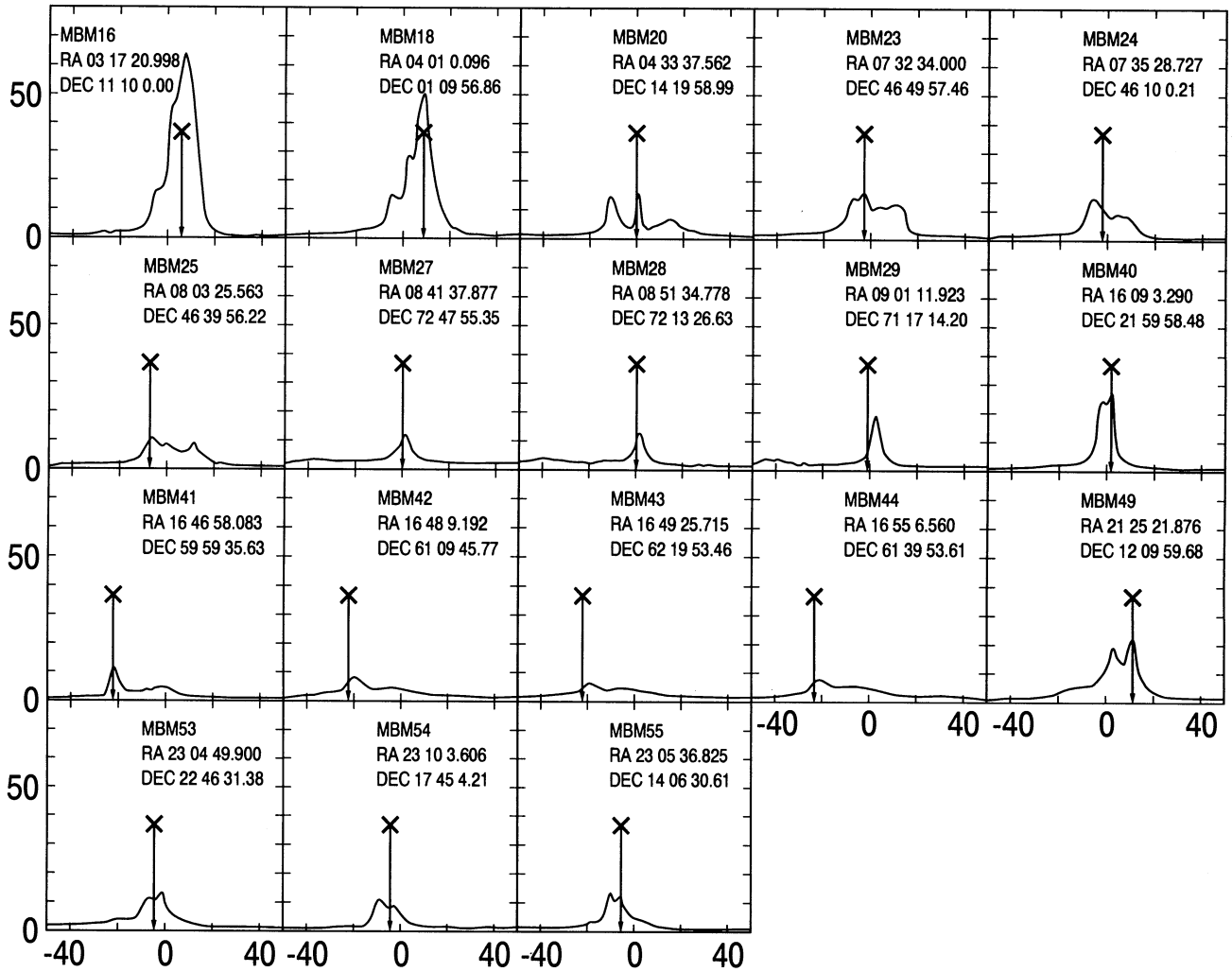

FIG. 2.—H I spectra at the positions of the CO peak of each HLC. The MBM cloud number and the CO peak position are marked at the top of each spectral map. The vertical line with an X indicates the corresponding V_{LSR} of the CO emission of each cloud. The scale of each panel is identical; the x-axis has a range of -50 km s^{-1} to $+50$ km s^{-1}, and the y-axis has a range of -1 K to 80 K.

simple velocity structure and the determination of how much H I is associated with the CO is therefore not always straightforward. In some cases, variations in the H I line profiles can also be found within the projected area of a cloud. However, the variation in the H I profiles is generally less within a cloud than it is from cloud to cloud. This can be seen in Figure 3 which shows the H I spectra in the immediate vicinity of the CO clouds. The clouds MBM 20, MBM 41–44 (the Draco clouds), and MBM 55 show the largest internal variations in the H I profile shapes.

We determine how much H I is associated with the molecular gas as follows. The H I spectra are fitted with 1–4 Gaussians depending on the profile. The component closest in velocity to the velocity centroid of the CO emission (in almost all cases, within 1–2 km s^{-1}) is chosen and the values derived for that Gaussian component over the area of the CO emission are averaged to produce a mean H I velocity centroid, V_{cent}, and a mean velocity dispersion, $\sigma(\text{H I})_{\text{LINEWIDTH}}$, for each cloud. The results are listed in Table 2. Also listed in this table are V_{LSR} and σ_{int}, the one-dimensional velocity dispersion of the CO clumps within a cloud; these are taken from MBM. We may think of σ_{int} as the dispersion of the ensemble of clumps within a cloud, which may be a reflection of the dispersion of the atomic gas from which the cloud formed. This quantity is equivalent to the σ_c parameter used by Dickman & Kleiner (1985) in their discussion of cloud turbulence. We also define $\sigma(\text{CO})_{\text{LINEWIDTH}}$ as the mean velocity dispersion within a particular CO clump. The quantity $\sigma(\text{CO})_{\text{LINEWIDTH}}$ is similar to the σ_i parameter defined by Dickman & Kleiner (1985). The latter values are taken from the observational results of MBM, Magnani (1987), and M. Pound (private communication).

We assume that the velocity interval of the H I associated with the CO cloud is just the full width at half-maximum, ΔV(H I), 2.35 times the $\sigma(\text{H I})_{\text{LINEWIDTH}}$ in Table 2, centered on the mean H I velocity. The H I within this velocity interval is integrated and plots of the resulting maps with the CO contours superposed onto them are shown in Figure 4 (Plates 7–16). The CO contour maps are taken from MBM. The accuracy with which the H I is associated with the CO depends upon how heavily blended the H I line profiles are. However,

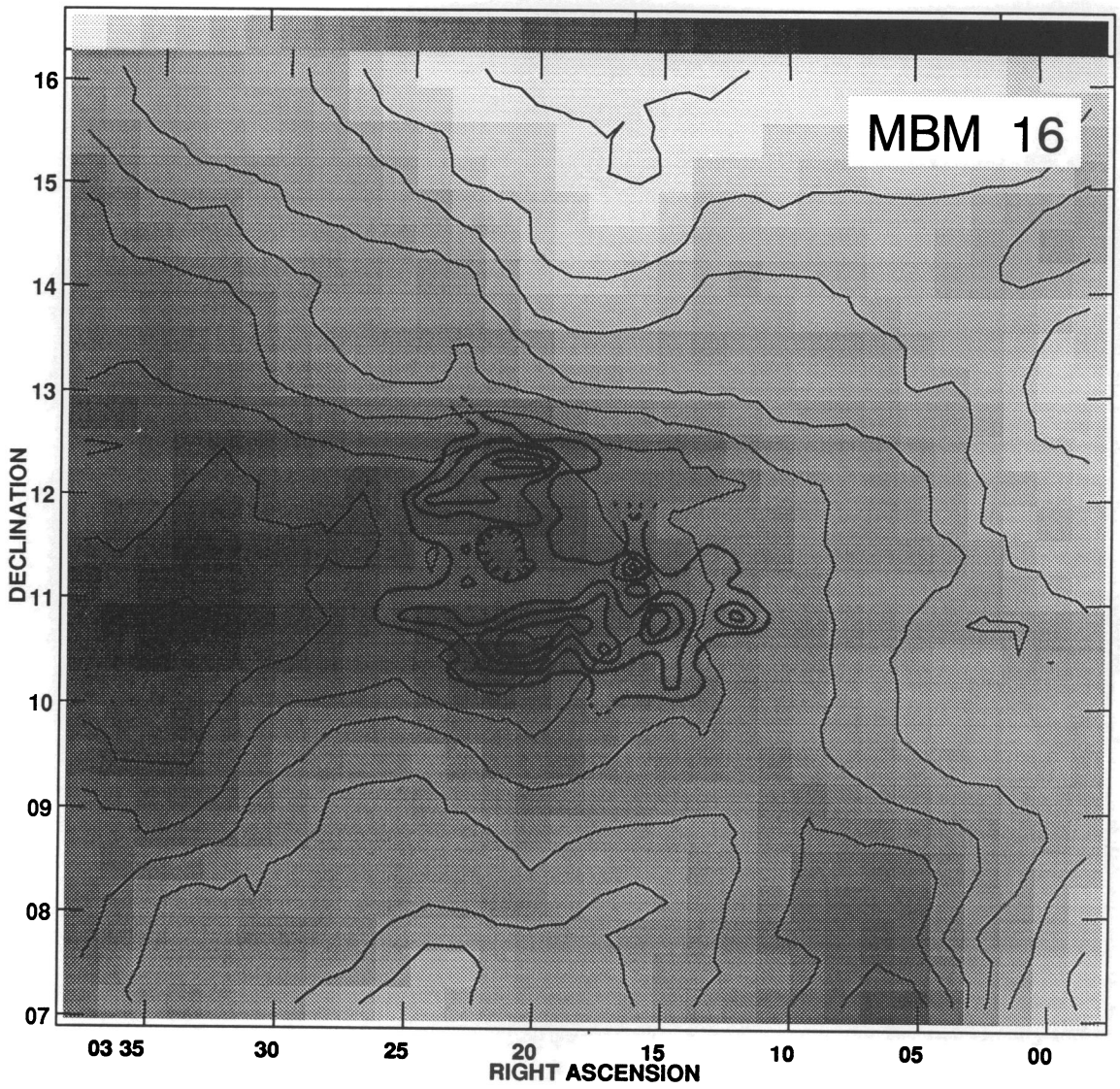

FIG. 4a

FIG. 4.—CO and H I contour maps of the HLCs and the associated H I gas. The CO contours were superposed onto the H I gray-scale contours with heavy lines. The CO contours were taken from MBM, with the lowest contour level 0.5 K and separated by 1 K. The H I data are Green Bank data. The contours and gray scales represent the intensity of the integrated antenna temperature. (*a*) The map of MBM 16. The first contour is 100 K km s^{-1}; the step level is 50 K km s^{-1}. The peak integrated intensity is 507 K km s^{-1}. (*b*) The map of MBM 18. The first contour is 160 K km s^{-1}; the step level is 20 K km s^{-1}. The peak integrated intensity is 398 K km s^{-1}. (*c*) The map of MBM 20. The first contour is 10 K km s^{-1}; the step level is 10 K km s^{-1}. The peak integrated intensity is 102 K km s^{-1}. (*d*) The map of MBM 23–24. The first contour is 80 K km s^{-1}; the level is 10 K km s^{-1}. The peak integrated intensity is 182 K km s^{-1}. (*e*) The map of MBM 25. The first contour is 50 K km s^{-1}; the step level is 10 K km s^{-1}. The peak integrated intensity is 78 K km s^{-1}. (*f*) The map of MBM 27–29. The first contour is 20 K km s^{-1}; the step level is 10 K km s^{-1}. The peak integrated intensity is 156 K km s^{-1}. (*g*) The map of MBM 40. The first contour is 120 K km s^{-1}; the step level is 10 K km s^{-1}. The peak integrated intensity is 195 K km s^{-1}. (*h*) The map of MBM 41–44. The first contour is 20 K km s^{-1}; the step level is 10 K km s^{-1}. The peak integrated intensity is 86 K km s^{-1}. (*i*) The map of MBM 49. The first contour is 50 K km s^{-1}; the step level is 10 K km s^{-1}. The peak integrated intensity is 98 K km s^{-1}. (*j*) The map of MBM 53–55. The first contour is 40 K km s^{-1}; the step level is 10 K km s^{-1}. The peak integrated intensity is 118 K km s^{-1}.

PLATE 8

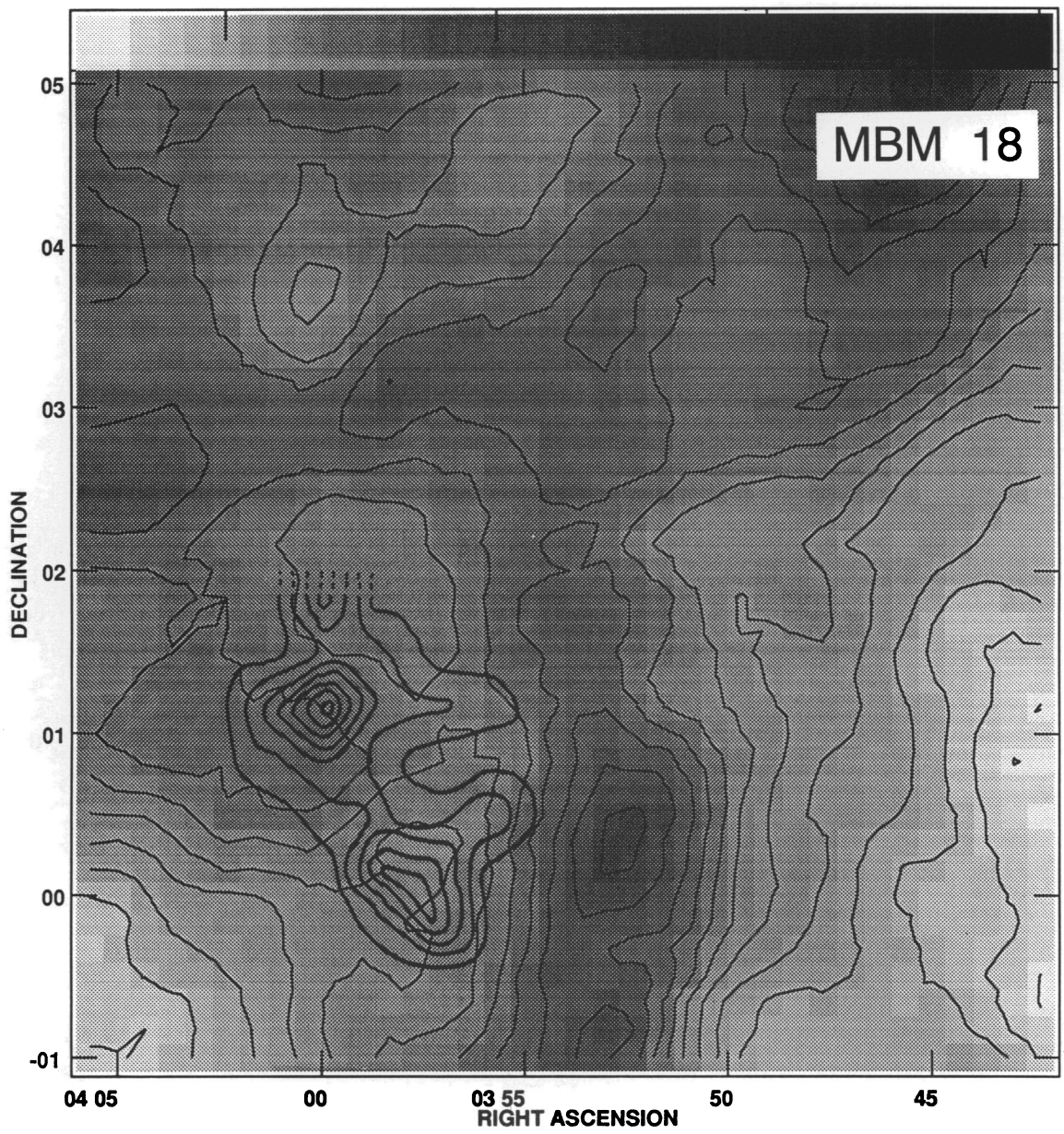

FIG. 4*b*

GIR, BLITZ, & MAGNANI (see 434, 164)

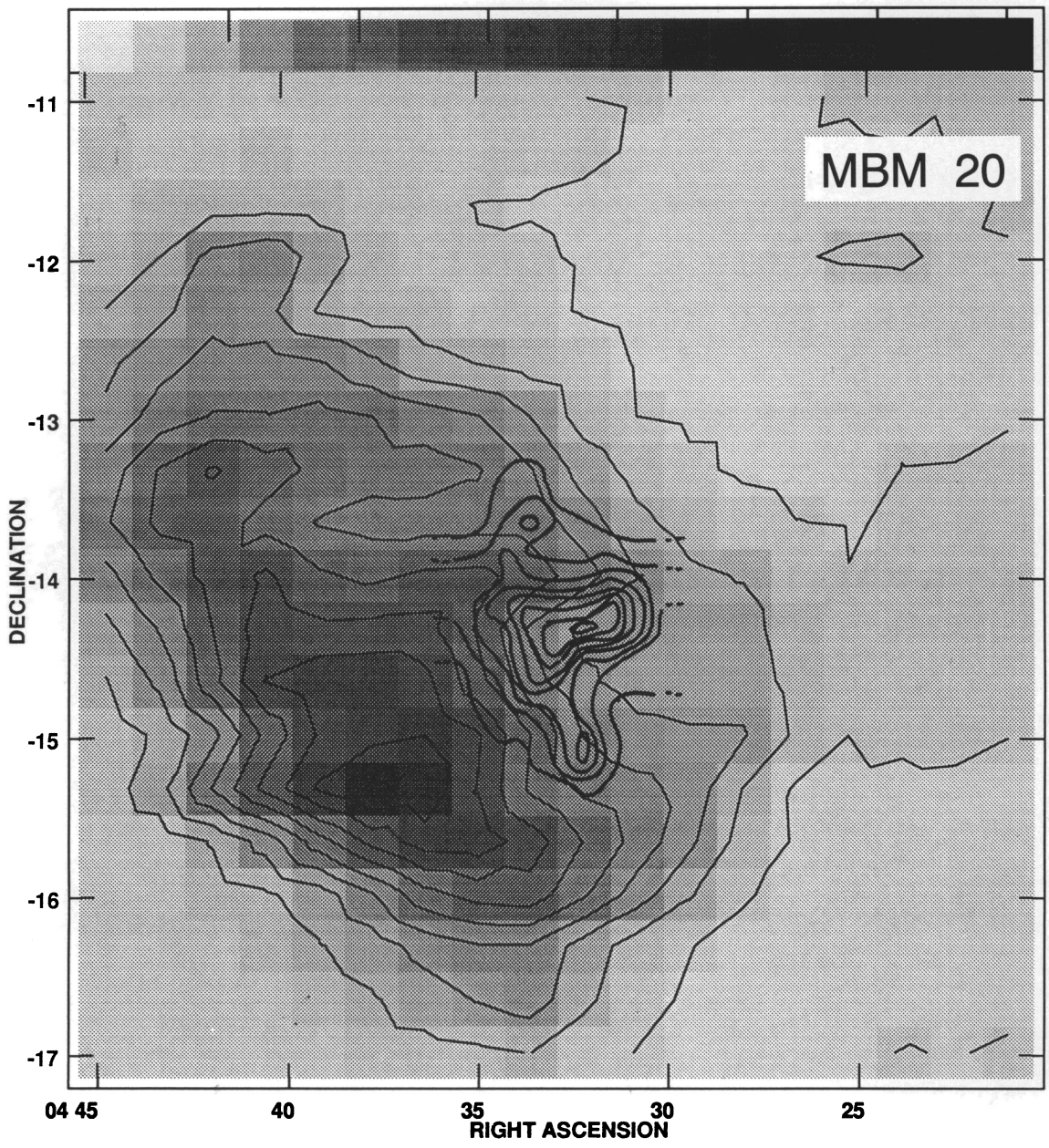

FIG. 4*c*

GIR, BLITZ, & MAGNANI (see 434, 164)

PLATE 10

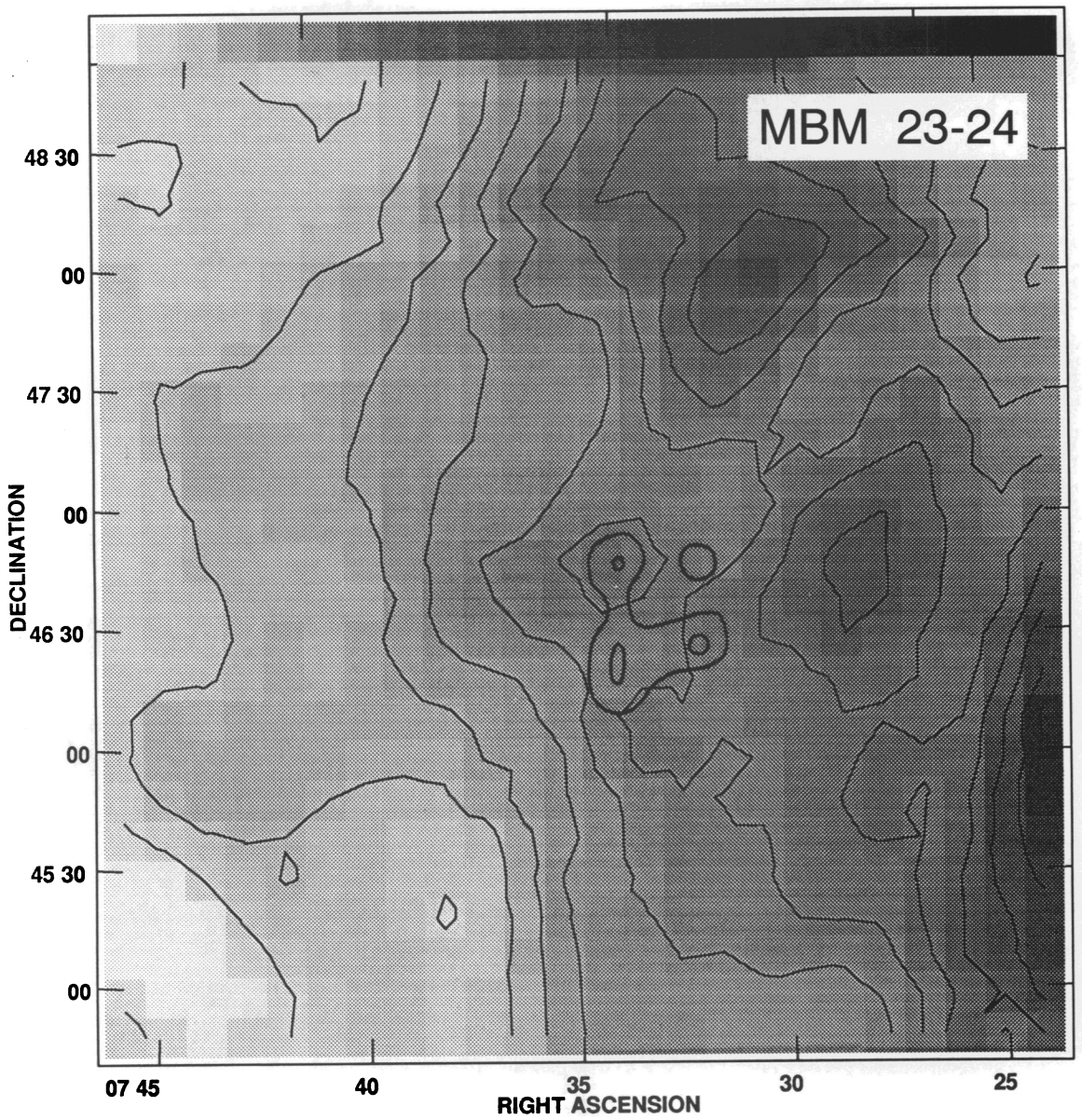

FIG. 4*d*

GIR, BLITZ, & MAGNANI (see 434, 164)

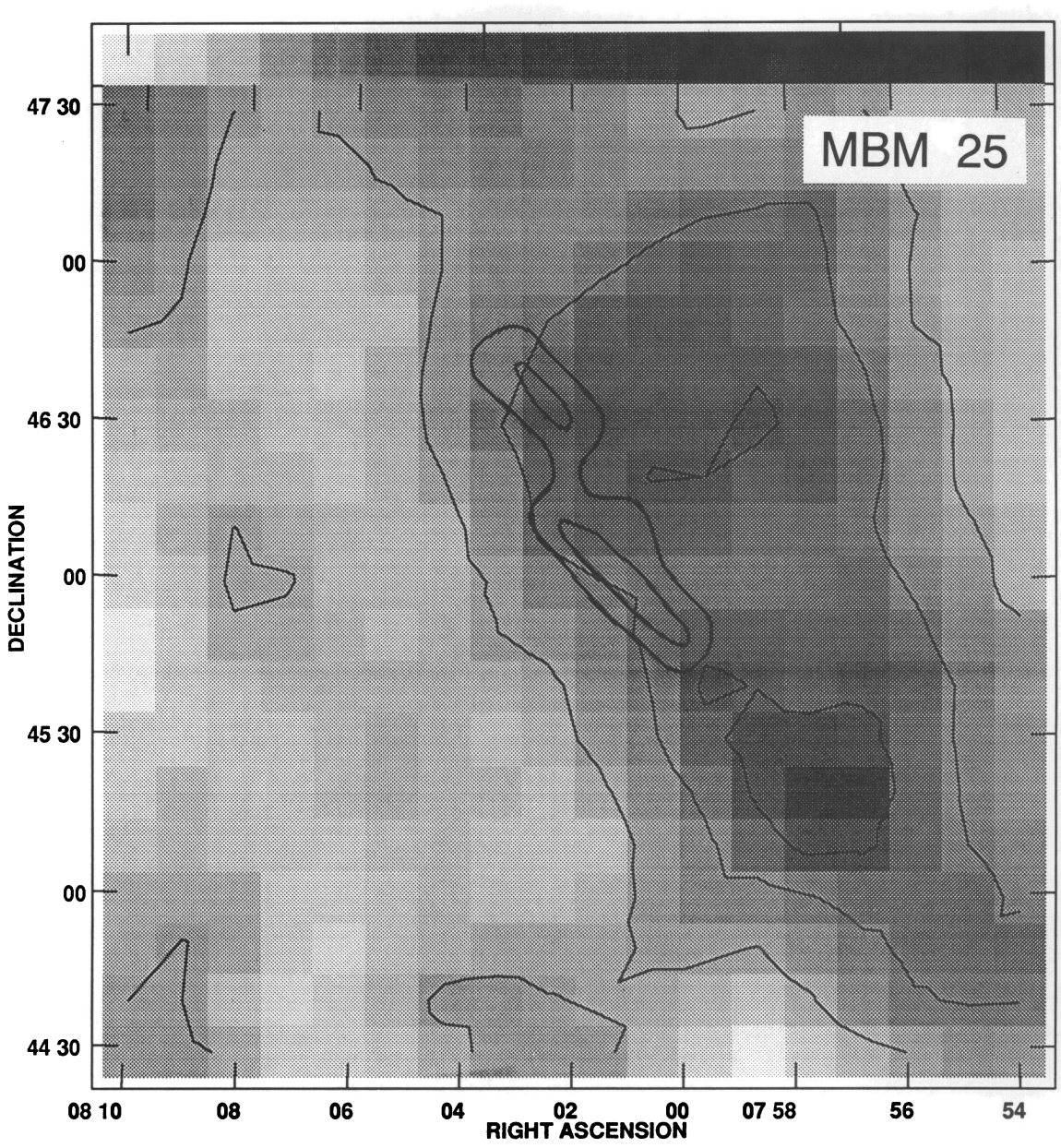

FIG. 4*e*

GIR, BLITZ, & MAGNANI (see 434, 164)

PLATE 12

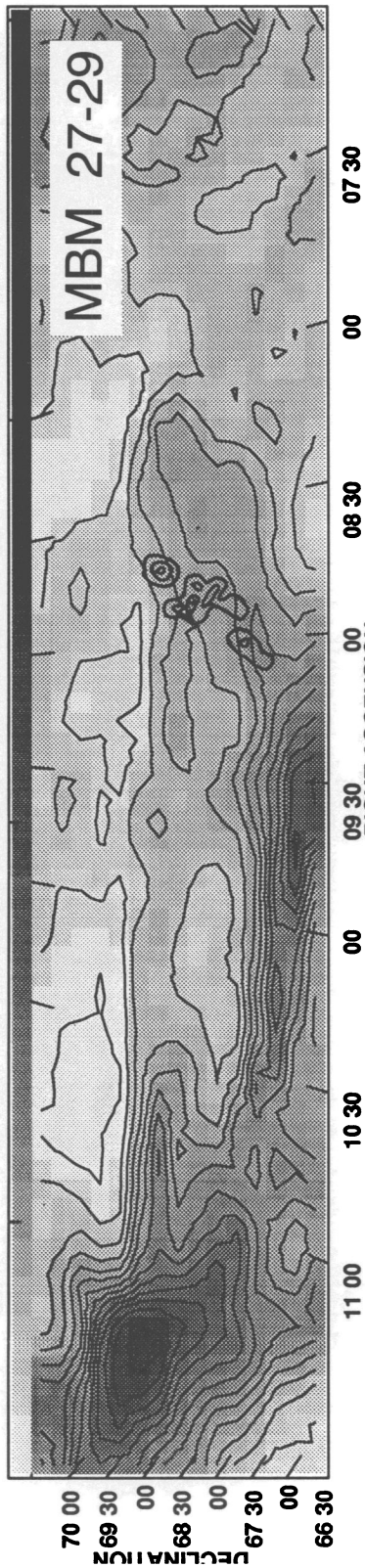

FIG. 4f

GIR, BLITZ, & MAGNANI (see 434, 164)

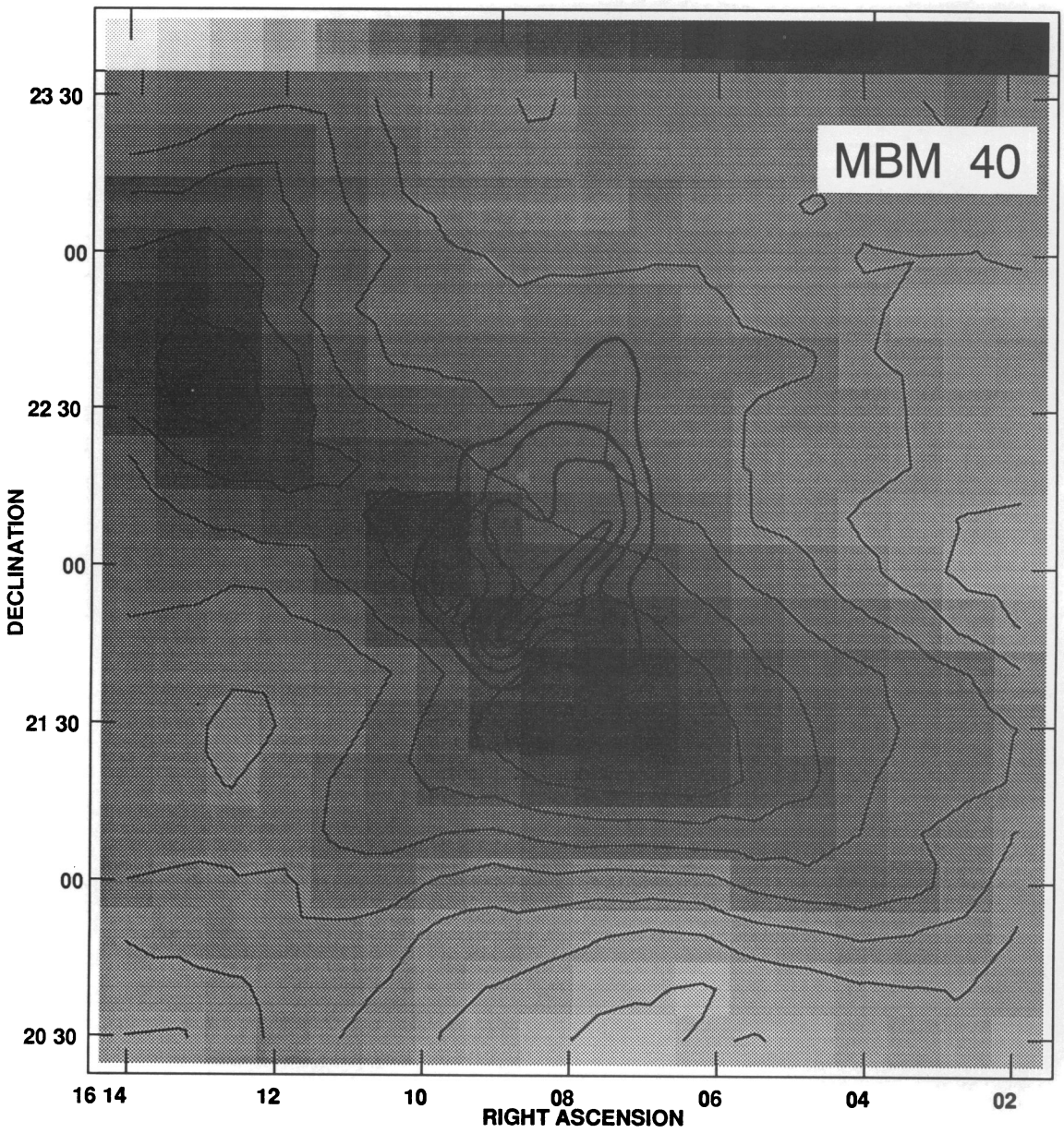

FIG. 4*g*

GIR, BLITZ, & MAGNANI (see 434, 164)

PLATE 14

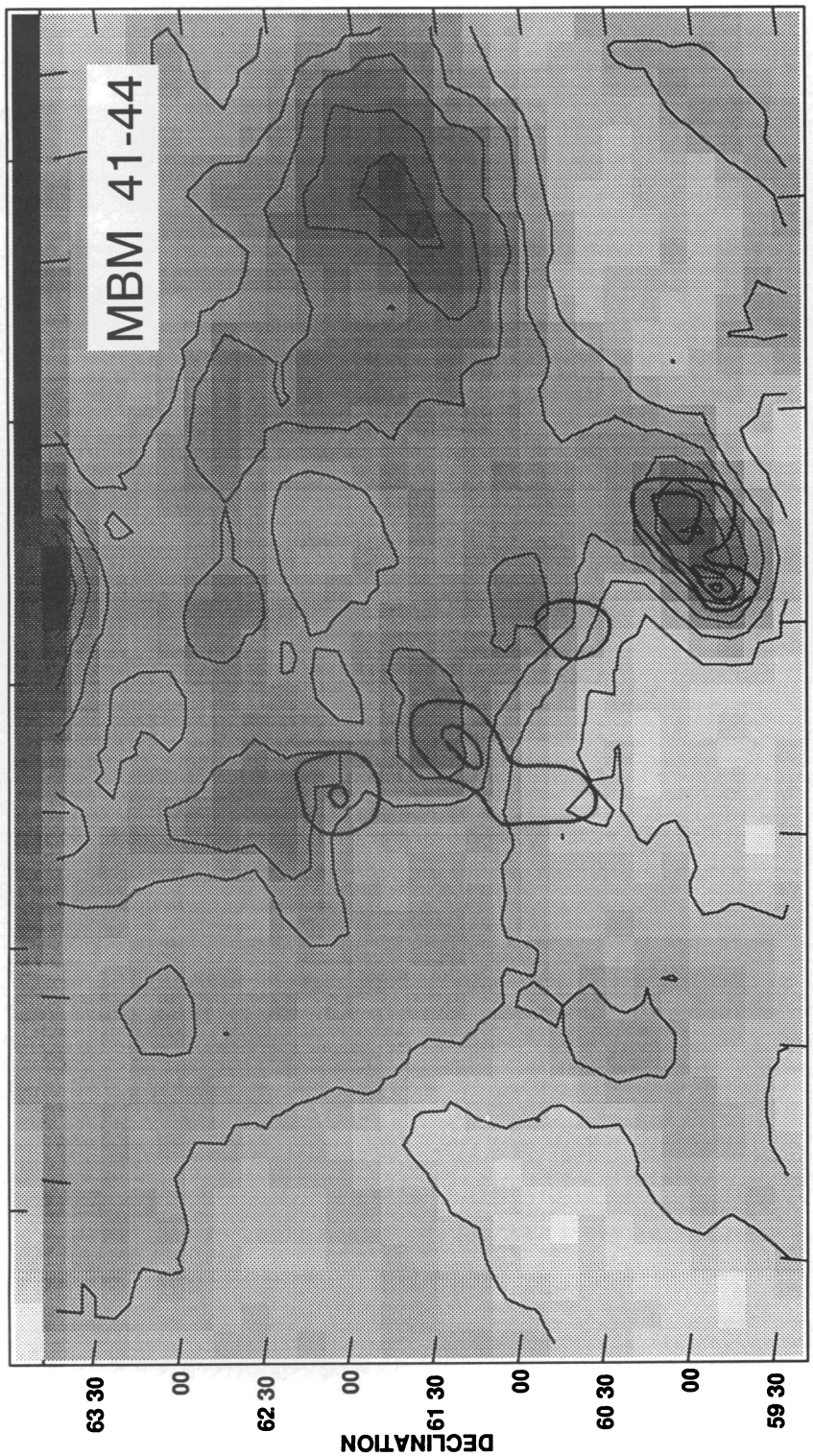

FIG. 4*h*

GIR, BLITZ, & MAGNANI (see 434, 164)

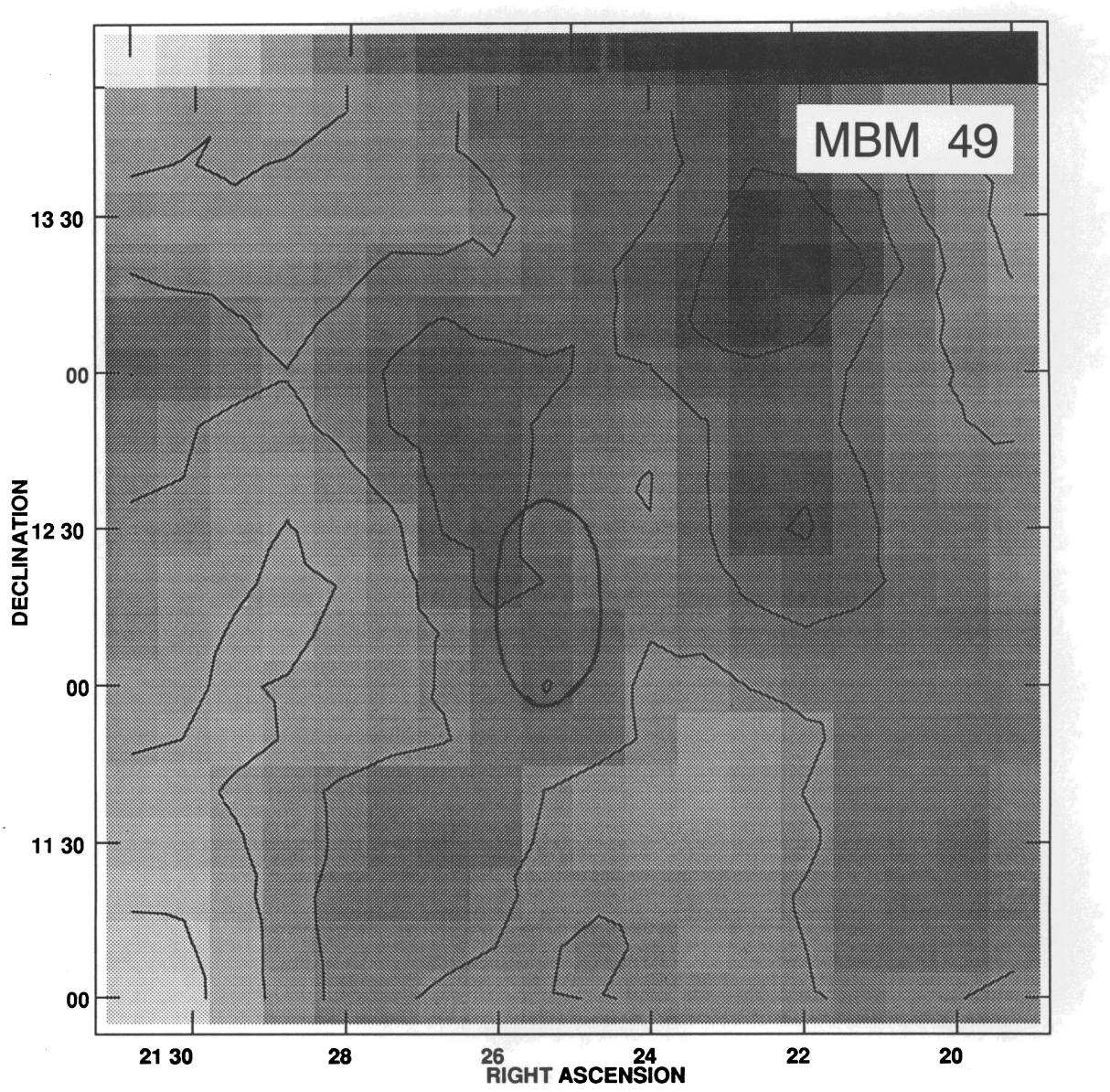

FIG. 4*i*

GIR, BLITZ, & MAGNANI (see 434, 164)

PLATE 16

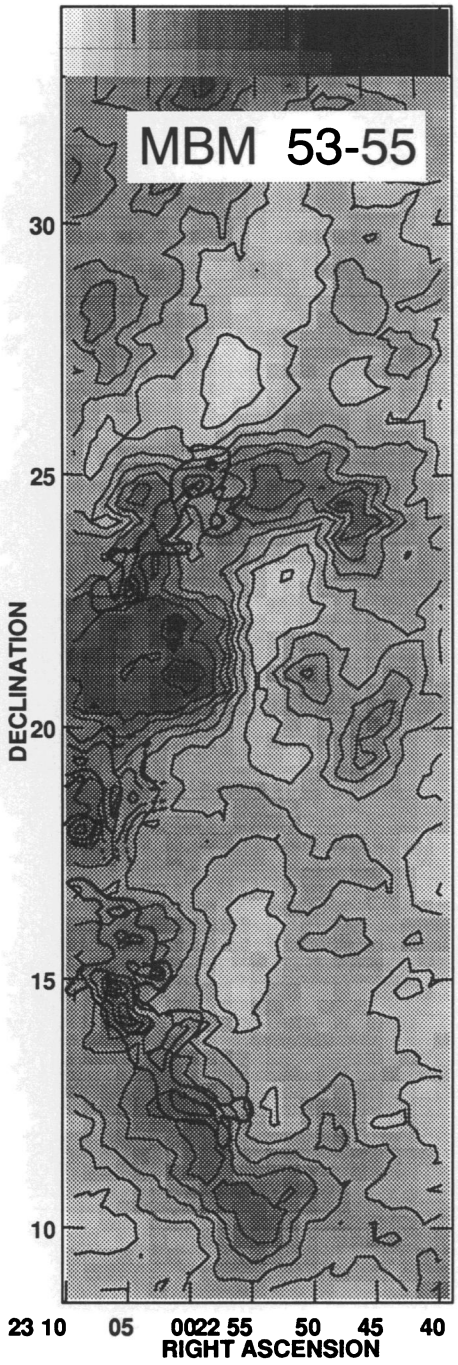

FIG. 4*j*

GIR, BLITZ, & MAGNANI (see 434, 164)

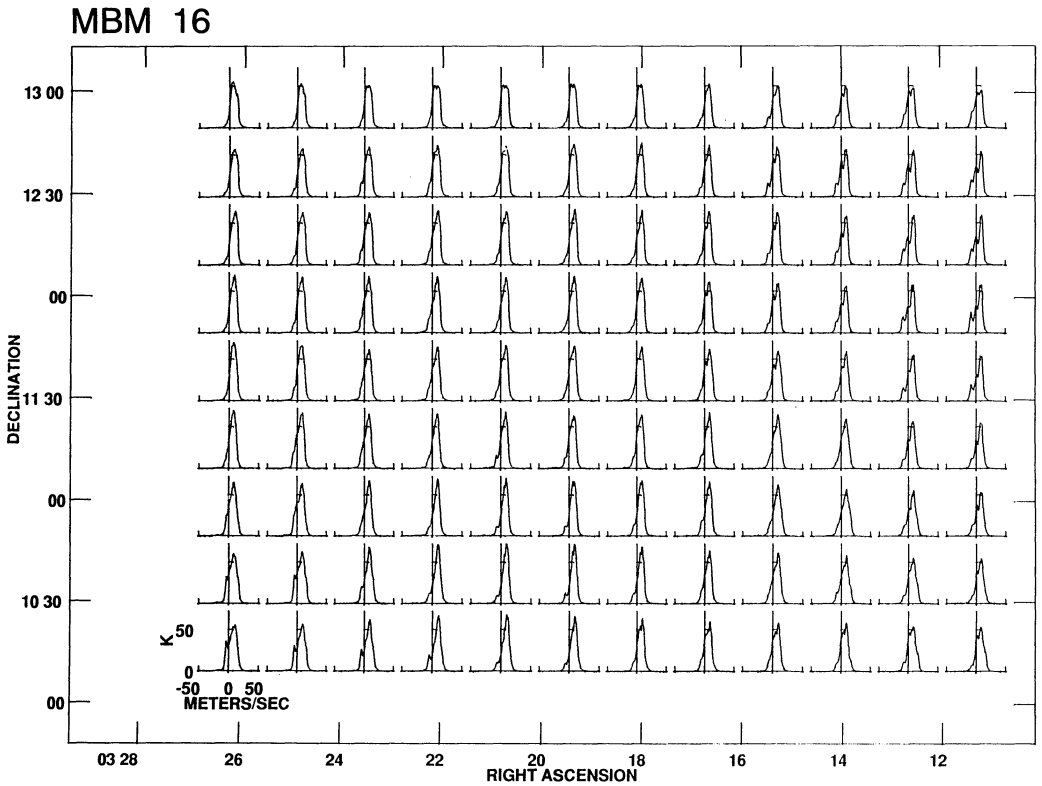

FIG. 3*a*

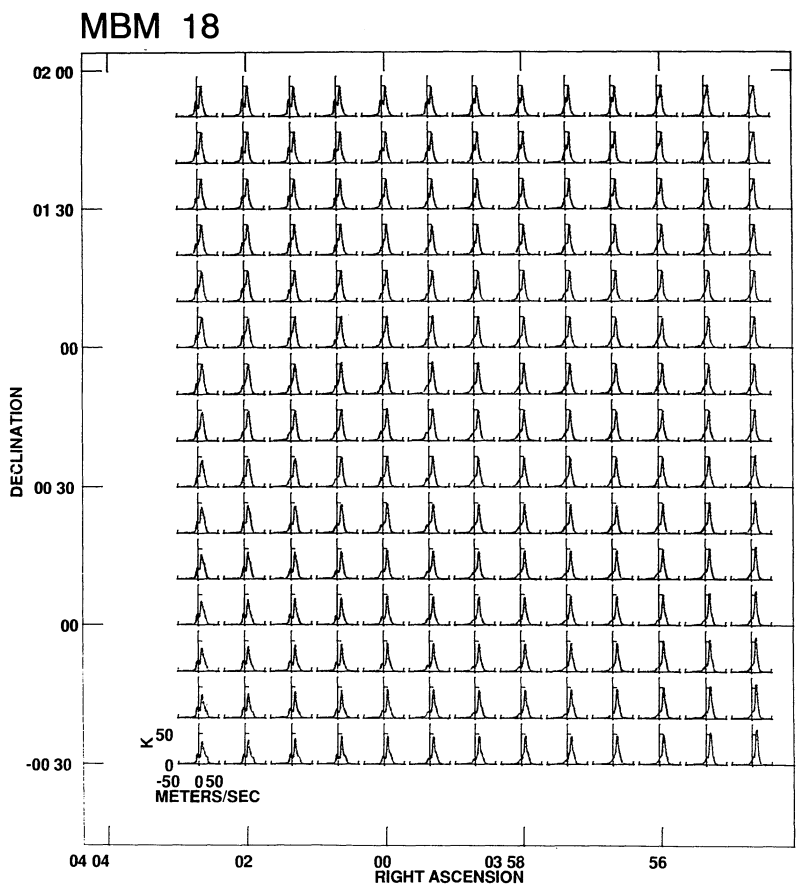

FIG. 3*b*

FIG. 3.—The H I spectra over each projected HLC area. The H I data are from Green Bank observations. The separation between spectra is equal to the observational sampling. The H I data for each cloud are generally much more extensive than what is shown in the figure.

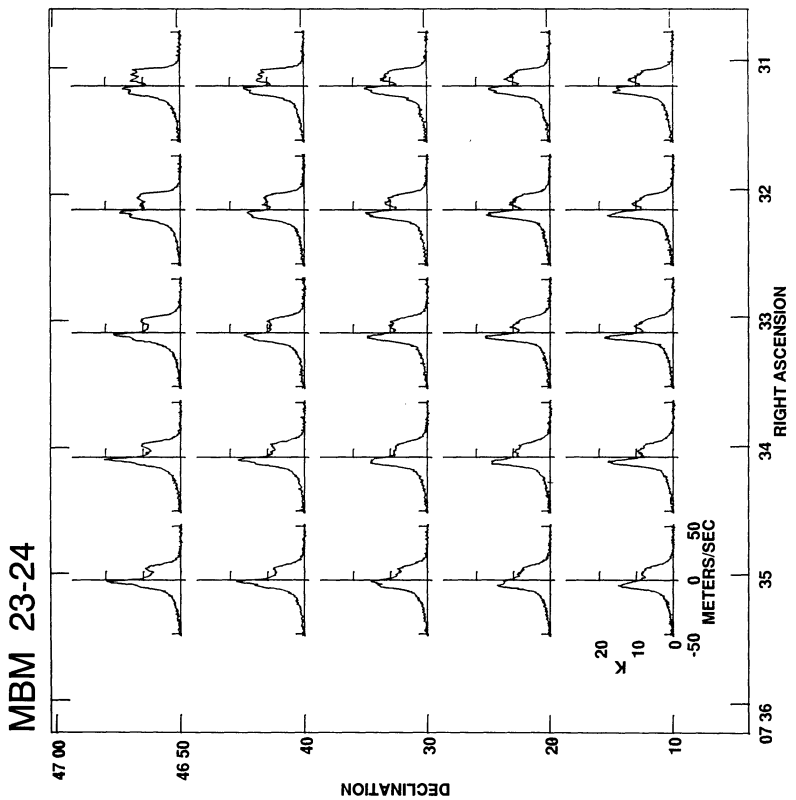

FIG. 3*d*

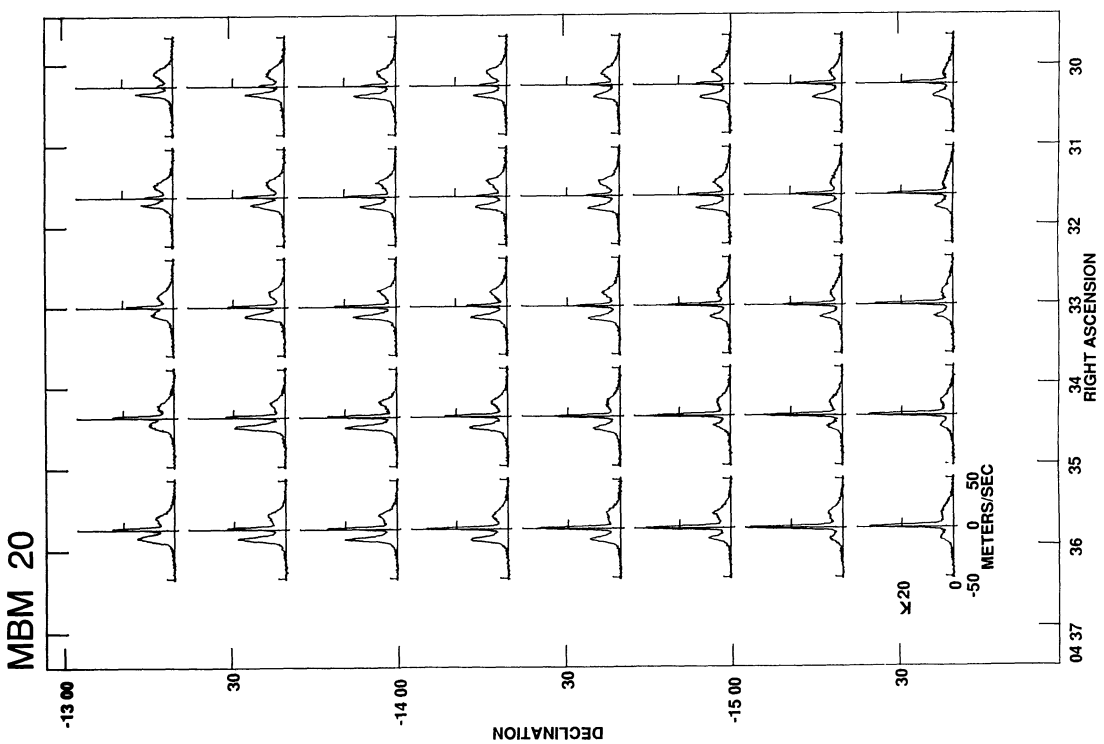

FIG. 3*c*

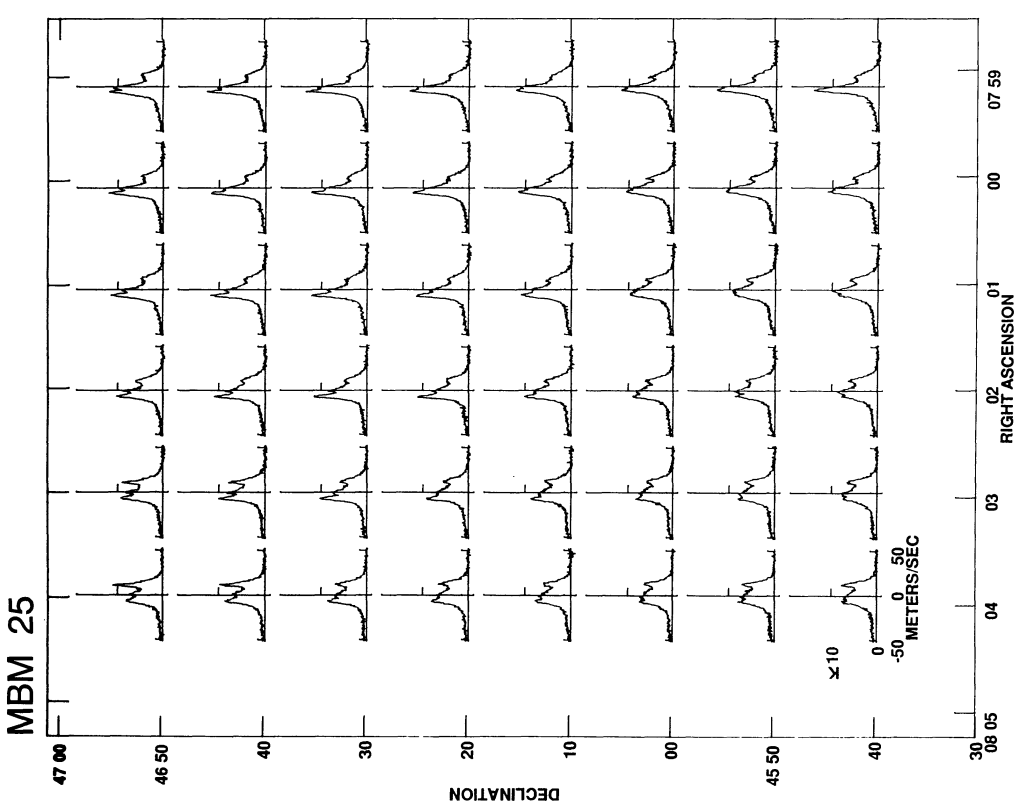

FIG. 3e

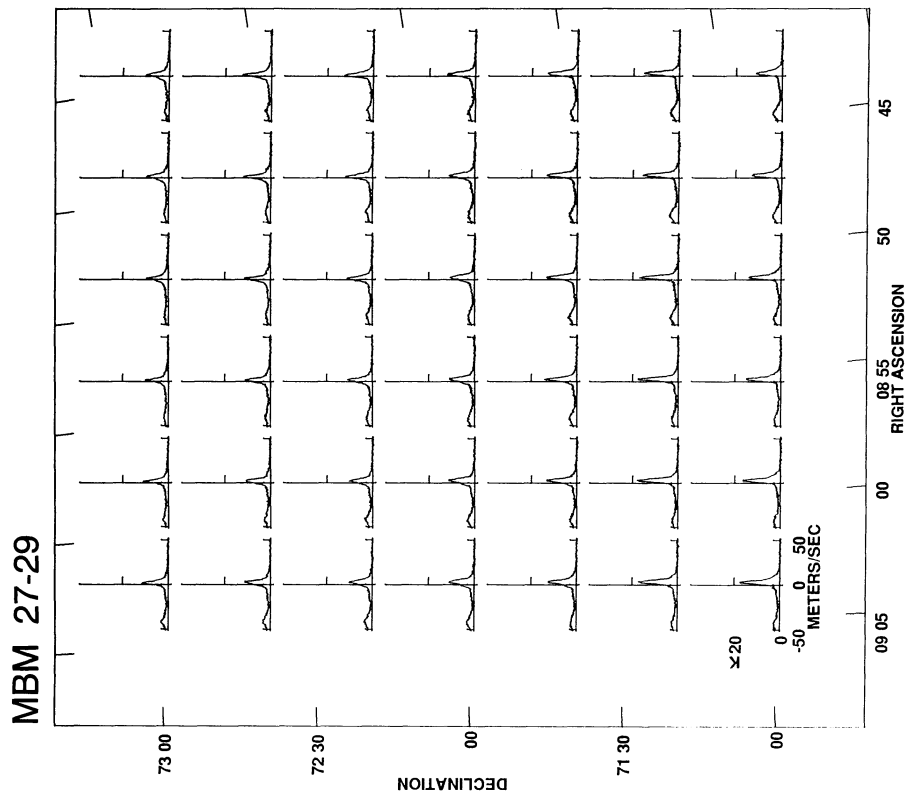

FIG. 3f

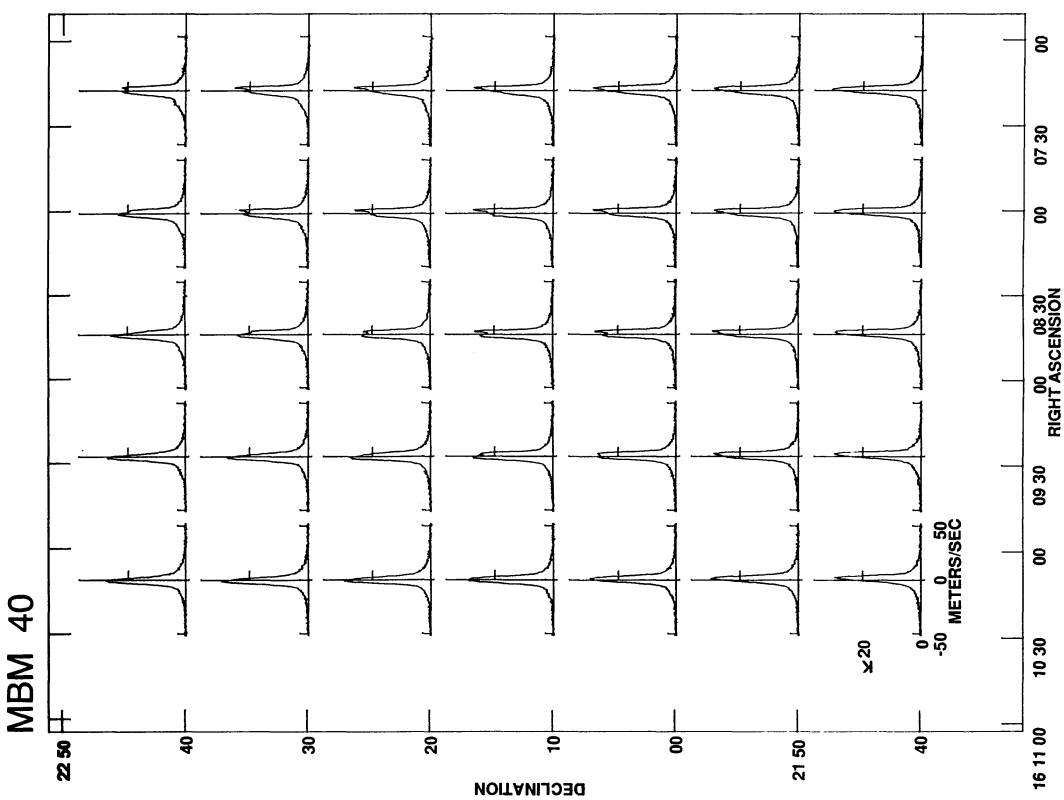

FIG. 3g

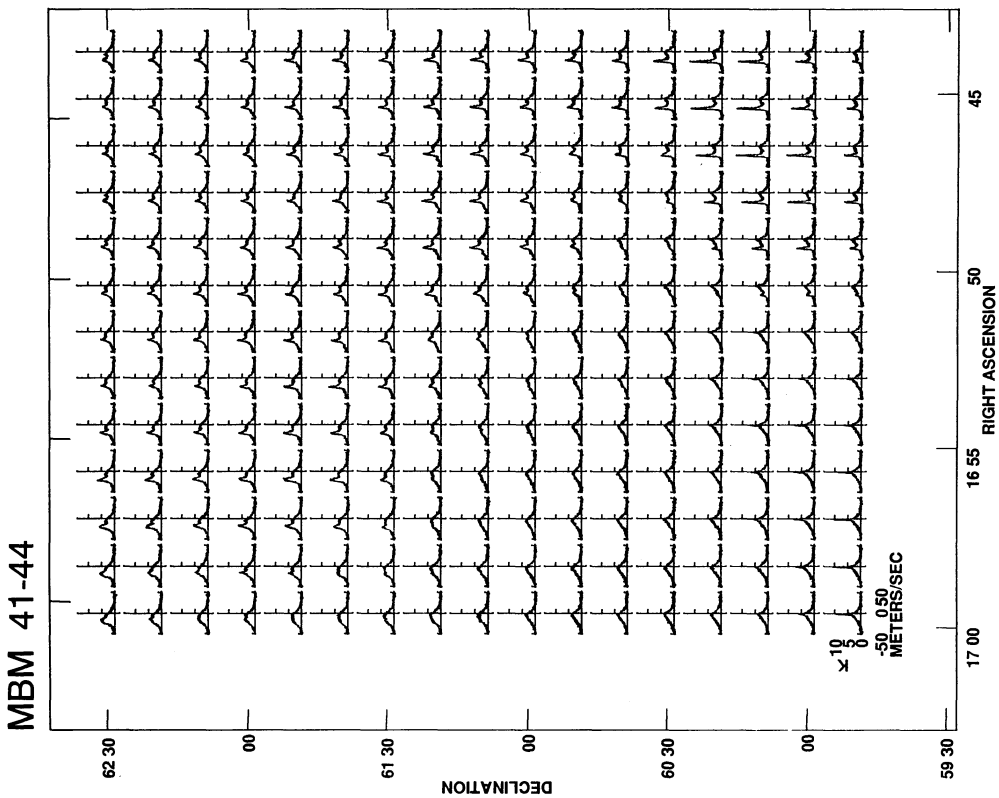

FIG. 3h

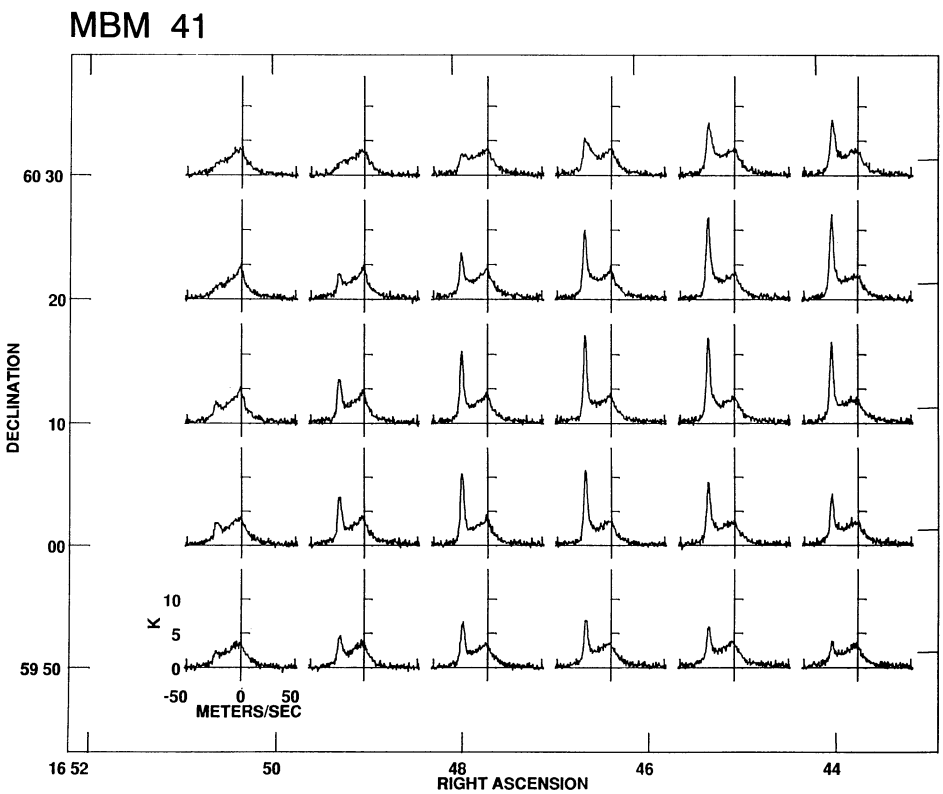

FIG. 3*i*

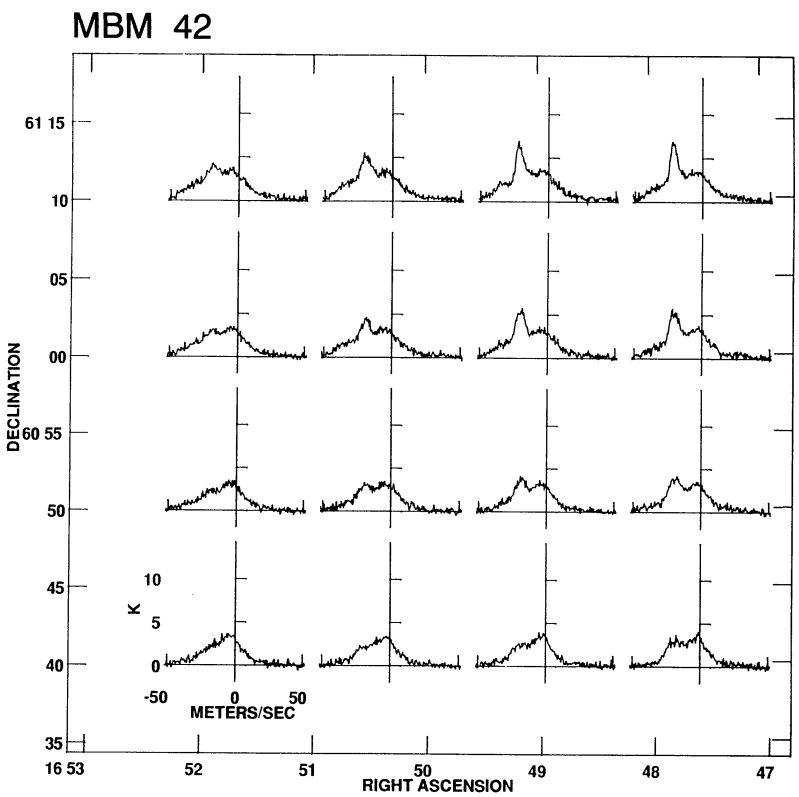

FIG. 3*j*

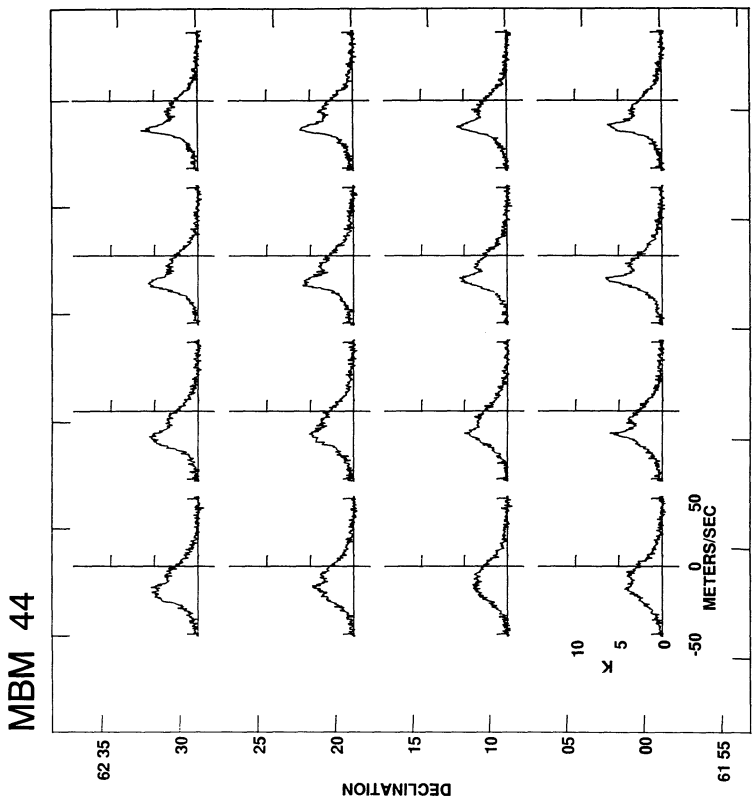

FIG. 3*l*

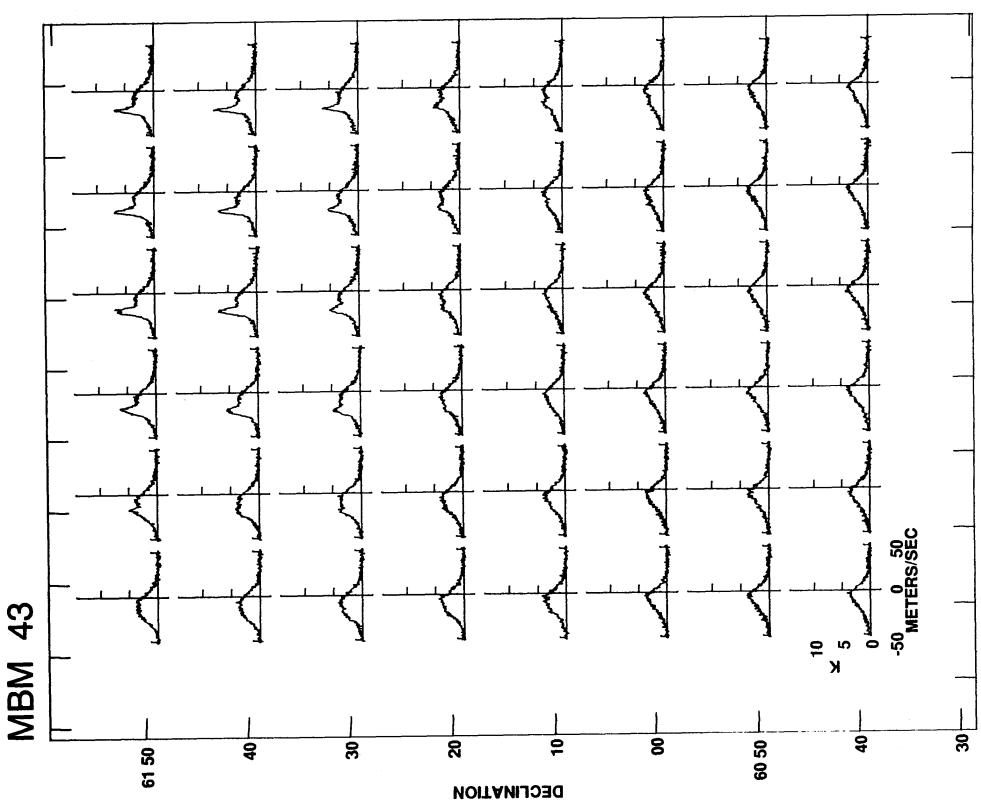

FIG. 3*k*

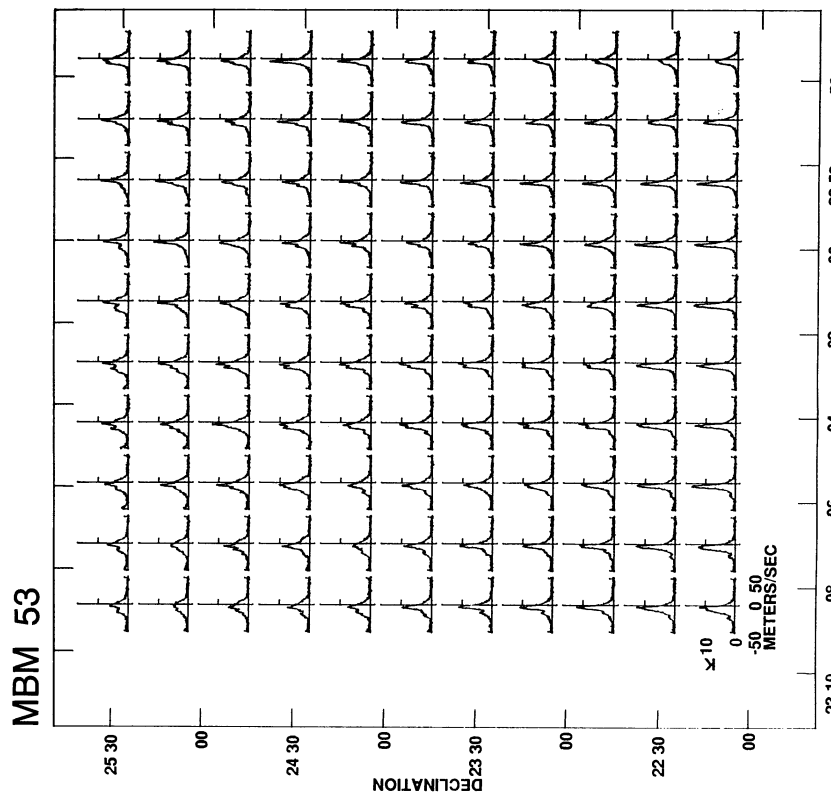

FIG. 3n

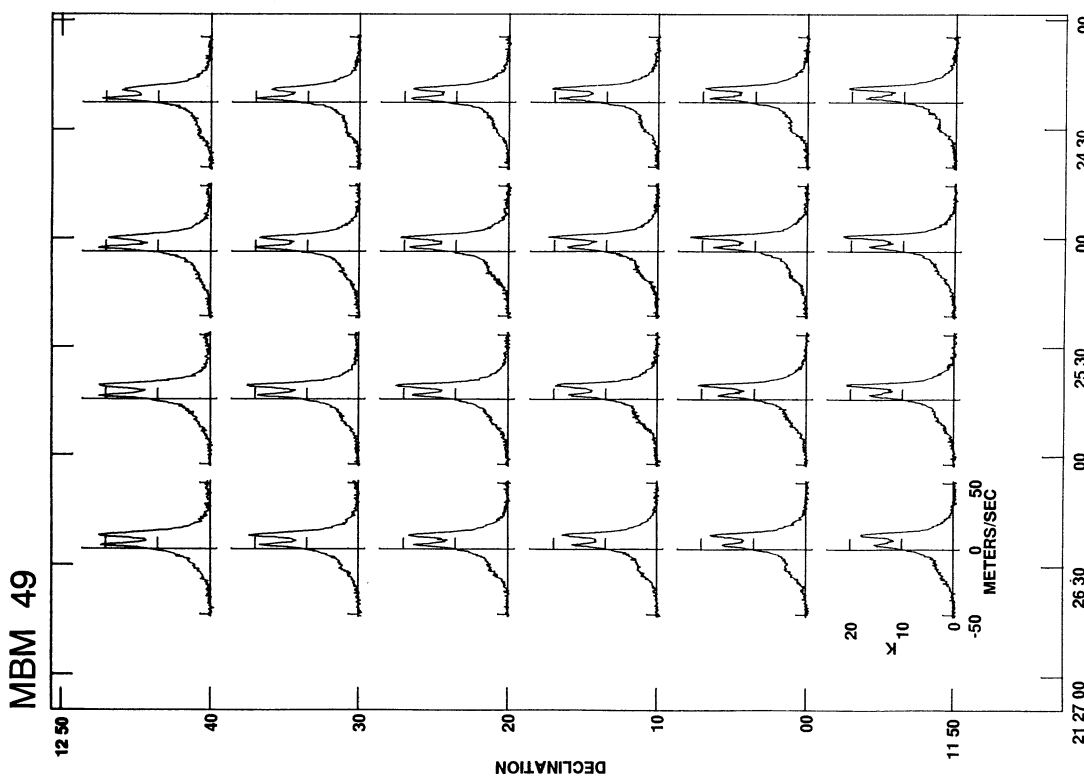

FIG. 3m

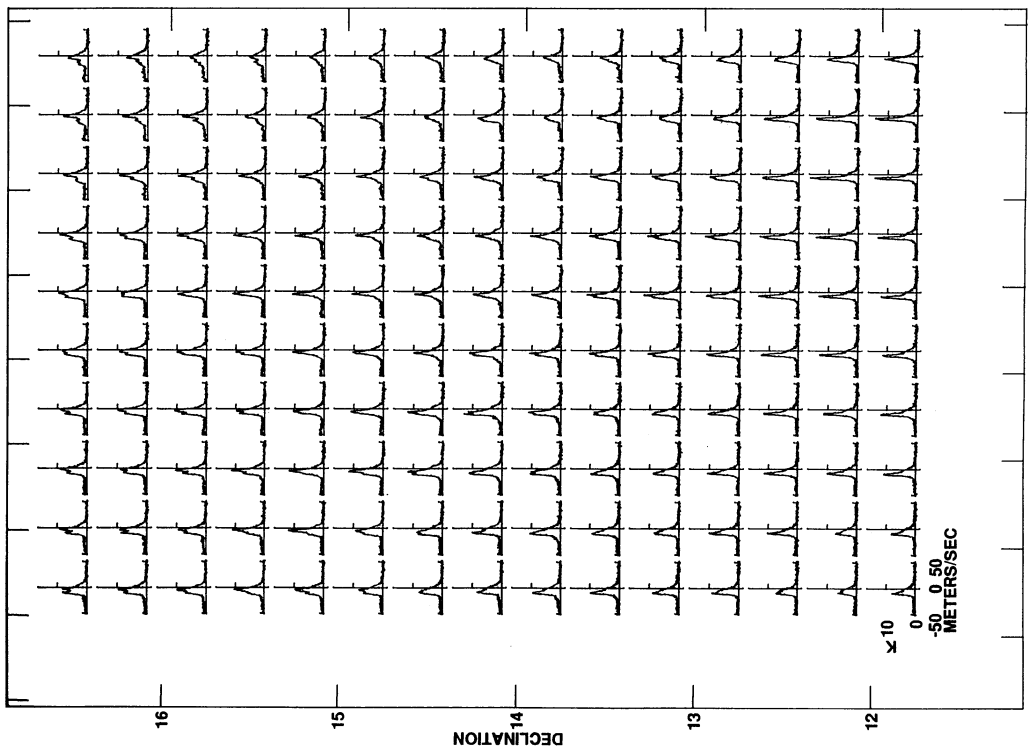

FIG. 3p

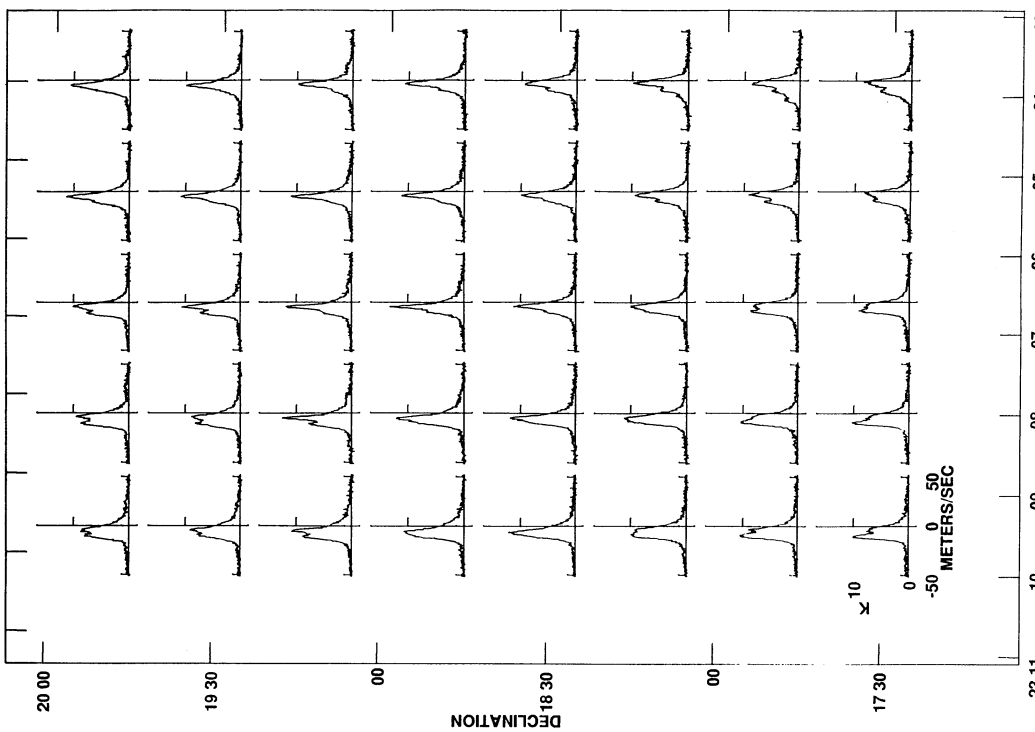

FIG. 3o

TABLE 2

CO AND H I SPECTRAL PARAMETERS

Clouds (MBM)	CO V_{LSR} (km s^{-1})	CO σ_{int} (km s^{-1})	CO $\sigma(CO)_{LINEWIDTH}$ (km s^{-1})	H I V_{cent} (km s^{-1})	H I $\sigma(H\ I)_{LINEWIDTH}$ (km s^{-1})
16	6.9	0.9	0.5	9.9	3.2
18	9.9	1.2	0.6	9.8	2.7
20	0.6	0.4	0.4	0.6	1.1
23	−1.7	0.9	0.9	−3.3	5.7
24	−1.7	0.9	0.9	−3.6	3.7
25	−8.1	0.6	0.4	−6.1	3.0
27	−0.1	2.0	0.6	0.9	1.7
28	−0.1	2.0	0.5	1.8	2.0
29	−0.1	2.0	0.8	2.7	1.6
40	3.2	0.3	0.3	0.4	3.0
41	−23.3	1.5	0.3	−22.5	1.9
42	−23.3	1.5	0.3	−18.9	3.0
43	−23.3	1.5	0.4	−20.0	4.0
44	−23.3	1.5	0.4	−19.3	3.3
49	11.0	0.8	0.7	9.5	1.9
53	−5.7	3.1	0.6	−4.9	3.5
54	−5.5	3.1	0.9	−6.0	4.3
55	−5.5	3.1	0.8	−6.6	3.9

small changes in the velocity interval used do not significantly affect the morphology of the H I maps.

It is worth noting that we created H I maps for all of the velocity components obtained after the Gaussian deconvolution of the H I spectra. In general, the maps of the different components look quite different from one another, suggesting that our procedure clearly separates the H I associated with an HLC from the foreground and background atomic gas.

3.2.2. CO-H I *Offsets*

Although some H I gas is invariably associated with the CO emission, it is immediately evident that substantial concentrations of H I are located adjacent to the clouds. thus, the overall impression from Figure 4 is that the CO peaks are offset from local H I maxima. In some clouds there are multiple H I peaks and the H I features have a morphology different from the associated CO clouds. In this paper, we define the H I peaks associated with the molecular clouds to be those peaks which are immediately adjacent to the cloud region. However MBM 27–29 is an exception to this definition. The MBM 27–29 complex is associated with an H I arclike feature which extends tens of degrees to the east and encompasses several other HLCs (e.g., de Vries, Heithausen, & Thaddeus 1987; Meyerdierks et al. 1991). Since no well-defined H I peaks are clearly identifiable near the MBM 27–29 molecular clouds within the area we mapped, we arbitrarily set the position of the H I peak at about $\alpha = 8^h40^m$, $\delta = +71°30'$, a location reasonably near the center of the H I filament in which the HLCs are embedded.

Table 3 lists this CO–H I offset and the effective diameter of the cloud, D_{eff}, which is defined as

$$D_{eff} = 2\left(\frac{\text{Projected area of the cloud}}{\pi}\right)^{1/2}, \quad (1)$$

The CO–H I offset varies from 0.°4 to 4.°0 with a mean value of 1.°5, which implies that the projected separation between the CO and H I peak is comparable to the mean linear diameter of the cloud. The implications of this offset will be discussed in § 4.

3.3. *Column Densities of* H_2 *and* H I

The determination of $N(H_2)$ from the CO emission is fairly straightforward; we use the conversion determined from the γ-ray data by Bloemen et al. (1986): $N(H_2) = 2.5 \times 10^{20} W(CO)$ cm^{-2}, where the value of $W(CO)$ is determined by $W(CO) = 2.35\sigma_{int} T_A^*$ K km s^{-1}. The quantity T_A^* is obtained directly from the CO contour map, and σ_{int} is the one-dimensional velocity dispersion of the cloud taken from MBM. Magnani, Blitz, & Wouterloot (1988) obtain a similar value for the $N(H_2)/W(CO)$ conversion factor for high-latitude clouds based on extinction data, CO observations, and a subset of the H I data presented in this paper, as do de Vries & van Dishoeck (1988) from optical observations of one line of sight through a translucent molecular cloud. On the other hand, recent studies of two HLCs (e.g., de Vries et al. 1987; Heithausen & Mebold 1989) suggest that for some high-latitude clouds, the $N(H_2)/W(CO)$ conversion factor may be

TABLE 3

CO–H I OFFSET AND CLOUD SIZE

Clouds (MBM)	Effective Diameter	CO–H I Offset
16	2.°6	4.°0
18	1.8	2.0
20	1.6	1.6
23	0.2	1.1
24	0.6	1.1
25	0.7	0.8
27	1.0	0.8
28	1.5	0.8
29	1.0	0.8
40	0.9	0.4
41	0.6	0.7
42	0.3	0.6
43	0.7	1.3
44	0.5	0.6
49	0.5	0.8
53	2.1	2.7
54	4.3	2.8
55	5.0	3.9

lower than the value we have used in this paper by as much as a factor of 6. The method employed by these authors, requires that the ratio of 100 μm surface brightness to total gas column density be a constant everywhere, an assumption known to be false for at least some clouds (e.g., Boulanger & Pérault 1988; Blitz 1991). Although we favor the higher conversion factor, most of the conclusions of this paper are not significantly affected if there is less H_2 relative to a given CO line brightness (see § 4.3).

For the atomic gas, we converted the 21 cm integrated antenna temperature to H I column density in the standard manner (e.g., Spitzer 1978) assuming that the H I emission is optically thin: $N(\mathrm{H\ I}) = 1.823 \times 10^{18} \int T_B\, dv\ \mathrm{cm}^{-2}$. The value of the integrated antenna temperature, $\int T_A\, dv$, is determined directly from the H I maps and is converted to $\int T_B\, dv$ using the beam efficiency $\eta_B = 0.8$. The optically thin assumption is valid for the vast majority of high-latitude molecular clouds because of the relatively low H I antenna temperatures. For each cloud, the H I peak column density refers to the column density at the position of the H I peak associated with the cloud as discussed above. The average column density of neutral gas over the cloud area defined by the CO contours and the mean total hydrogen column density is simply obtained from $\langle N(\mathrm{H_{total}})\rangle = \langle N(\mathrm{H\ I})\rangle + 2\langle N(\mathrm{H_2})\rangle$. Table 4 lists these column densities. Since these column densities are related to the positions of the highest emission and the cloud area, the tabulated values may be somewhat sensitive to the resolution and sampling of the CO and H I data.

In spite of the care we have taken to identify only the H I associated with a particular HLC, the H I column density listed in Table 4 may still contain some small contribution from background emission. For example, Verschuur & Schmelz (1989) and Verschuur & Magnani (1994) argue that, in general, there exists a broad, low-intensity H I component unrelated to sidelobe contamination, present in most lines of sight. The broad component (referred to as "Component 2" in those papers can be seen in some of the spectra shown in Figure 2 and is probably associated with the warm neutral medium (see review by Kulkarni & Heiles 1987). For the most part, the contribution of Component 2 to the H I column densities in Table 4 is less than 20% of the tabulated values and in many cases is much smaller. We therefore ignore the contribution of this component in the following discussion.

TABLE 4

ATOMIC AND MOLECULAR COLUMN DENSITIES

Clouds (MBM)	$N(\mathrm{H\ I})_{peak}$ (10^{20} cm^{-2})	$\langle N(\mathrm{H\ I})\rangle$ (10^{20} cm^{-2})	$\langle N(\mathrm{H_2})\rangle$ (10^{20} cm^{-2})	$\langle N(\mathrm{H_{total}})\rangle$ (10^{20} cm^{-2})
16.....	11.6	9.3	4.9	19.1
18.....	8.8	6.4	9.4	25.2
20.....	2.3	1.2	4.5	10.2
23.....	3.5	2.9	2.5	7.9
24.....	3.5	2.9	2.7	8.3
25.....	1.6	1.4	2.1	5.6
27.....	1.7	1.1	7.5	16.1
28.....	1.7	1.2	7.2	15.6
29.....	1.7	1.5	6.7	14.6
40.....	4.4	3.9	2.4	8.7
41.....	1.6	1.0	7.4	15.8
42.....	1.2	0.8	4.4	9.6
43.....	1.3	0.7	4.9	10.5
44.....	1.4	1.0	4.5	10.0
49.....	2.0	1.8	2.3	6.4
53.....	2.7	1.8	12.6	27.0
54.....	2.7	1.9	15.5	32.9
55.....	2.3	1.9	11.5	24.9

3.4. H I *Filaments and Expanding Shells*

From the velocity channel maps of the Green Bank H I data, it is evident that two of the 10 mapped regions. MBM 27–29 and MBM 53–55, show clear arclike structures (see Fig. 5). This figure was created by averaging the H I data over 11 velocity channels (about 5.7 km s^{-1}) centered at V_{cent} of each complex (see Table 2). These arclike H I features suggest that previous energetic events such as supernova explosions or stellar winds have taken place and have swept up the gas shell-like configurations. As a result of the explosions, these shells may still be expanding at present. An expanding shell will show a changing radius of curvature as a function of velocity. In addition, evidence of such an expansion may be obtained by comparing channel maps at different velocities, or by displaying in rapid succession a series of sequential velocity channel maps (i.e., a "movie") on a computer screen. Both methods were employed to determine if the shell structure is expanding.

Although the channel maps in MBM 27–29 look as if the arclike feature has a changing radius of curvature (see Fig. 6*a*) the rapid display of the channel maps suggests a more complex picture and a more ambiguous interpretation. The situation for MBM 53–55 is also complex, but the interpretation is less ambiguous. Figure 6*b* shows two filamentary arcs, which may even be interacting. The brightest portion of the H I map is located at the intersection of these two arcs. The more southerly of the two arcs, seen in velocity channels $V = -11.3$ to -3.6 km s^{-1}, does show a clearly varying radius of curvature both in the "movie" and in the channel maps; the more northerly arc is seen in velocity channels $V = -16.5$ to -12.9 km s^{-1} and shows no apparent expansion. The feature at $\alpha = 22^{\mathrm{h}}48^{\mathrm{m}}$, $\delta = +20°$ in the $V = -2.1$ km s^{-1} and $V = 1.0$ km s^{-1} panels looks as if it could be the rearmost section of the shell. Because the interpretation of MBM 27–29 as an expanding H I shell is ambiguous with our data set, we consider only MBM 53–55.

We begin by considering a uniformly expanding, nonrotating shell. For a given observed angular radius θ, and velocity V_{obs}, a ringlike structure would be seen by an observer at the origin. V_{center} is the systemic velocity of the shell along the line of sight toward the shell center, V_{exp} is the shell expansion velocity, and the quantities ψ and ϕ are defined as shown in Figure 7. Note that for the shell considered here, r is not negligibly small compared to d. We thus have

$$V_{obs} = V_{center} \cos\theta + V_{exp} \cos\psi\ , \qquad (2)$$

where V_{obs}, V_{center}, and V_{exp} are defined as above. From geometry, the above equation can be rewritten as

$$V_{obs} = V_{center} \cos\theta \pm V_{exp}\left[1 - \left(\frac{d}{r}\right)^2 \sin^2\theta\right]^{1/2}\ , \qquad (3)$$

where d and r are the distance and radius of the shell respectively, and the "+" and "−" signs refer to the half of the shell expanding away from and toward the observer, respectively. The quantity d is known from absorption-line measurements to foreground and background stars in the direction of the clouds to be 200 ± 50 pc (Welty et al. 1989). The quantity r can be obtained under the assumption that the largest angular

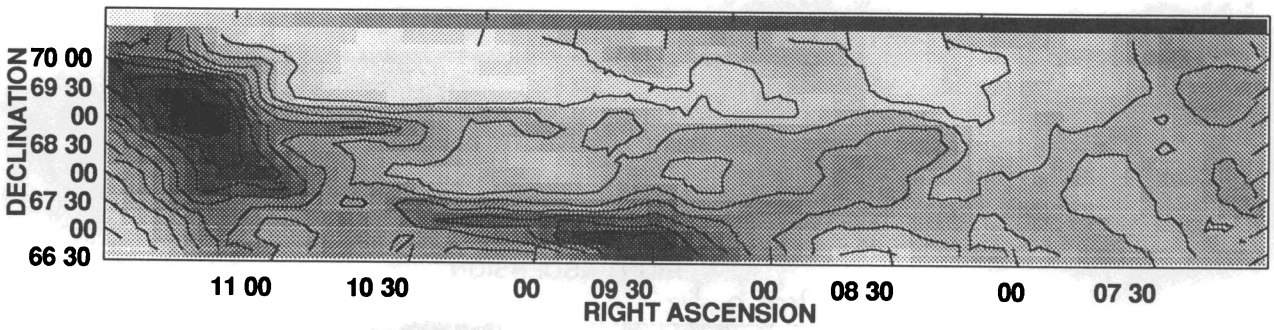

FIG. 5a

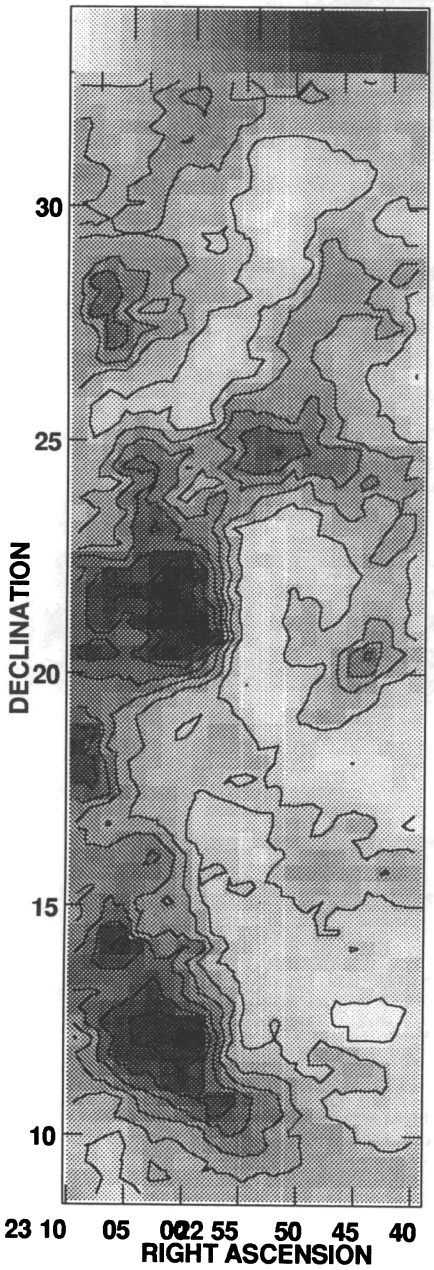

FIG. 5b

FIG. 5.—H I shell-like structures of the MBM 27–29 and MBM 53–55 regions. Each map is averaged over 11 velocity channels and centered at the corresponding V_{LSR} of the CO. (*a*) For MBM 27–29 panel, the lowest contour is 5 K km s^{-1} and the contour separation is 5 K km s^{-1}. (*b*) For MBM 53–55 panel, the lowest contour is 2 K km s^{-1} and the contour separation is 2 K km s^{-1}.

diameter subtended by the shell is tangent to the line of sight. If this assumption is incorrect, we obtain only a lower limit to the expansion velocity, but the error is likely to be small. Because the quantities in the brackets in equation (3) are known, the expansion velocity can be obtained from a simple linear regression.

Table 5 gives the measured angular diameters of the more southerly arc of the MBM 53–55 H I shell in the velocity channels where the measurements are unambiguous. The measurements are made along the ridge line of the filaments. The quantity V_{obs} is plotted against $[1 - (d/r)^2 \sin^2 \theta]^{1/2} = \cos \psi$ in Figure 8. We obtain an expansion velocity for the shell of 18 km s^{-1} and a value for V_{center} of -12 km s^{-1} from the fit to the data. If the feature at $\alpha = 22^h48^m$, $\delta = +20°$ indicated in Figure 6*b* (*left-hand panel*) does indeed represent the back part of the expanding shell, then the shell expansion velocity is determined approximately but directly by the difference between the velocity of the back portion and the velocity of the maximum extent of the shell. The implied expansion velocity is about 10–13 km s^{-1}, in rough agreement with the fit.

Although our H I data in the vicinity of some of the clouds that make up the Ursa Major complex (MBM 27–32) were insufficient to determine an expansion velocity, Meyerdierks et al. (1991) performed an analysis of other data and found the H I shell to be expanding at a rate of about 20 km s^{-1}, a value similar to that found for the MBM 53–55 H I shell.

In addition to the above examples, we also note a recent paper by Burrows et al. (1993) which identifies a shell of neutral material around the Eridanus soft X-ray enhancement. The

TABLE 5

ANGULAR DIAMETERS OF MBM 53–55 H I SHELL AT VARIOUS VELOCITY CHANNELS

Channel Velocity (km s^{-1})	Angular Diameter
−11.1	17°.8
−10.6	17.6
−10.0	17.8
−9.5	17.4
−9.0	17.6
−8.5	17.6
−8.0	18.0
−7.5	17.4
−7.0	17.2
−6.4	17.0
−5.9	16.6
−5.4	16.8
−4.9	16.8
−4.4	16.4
−3.9	17.0
−3.3	16.4

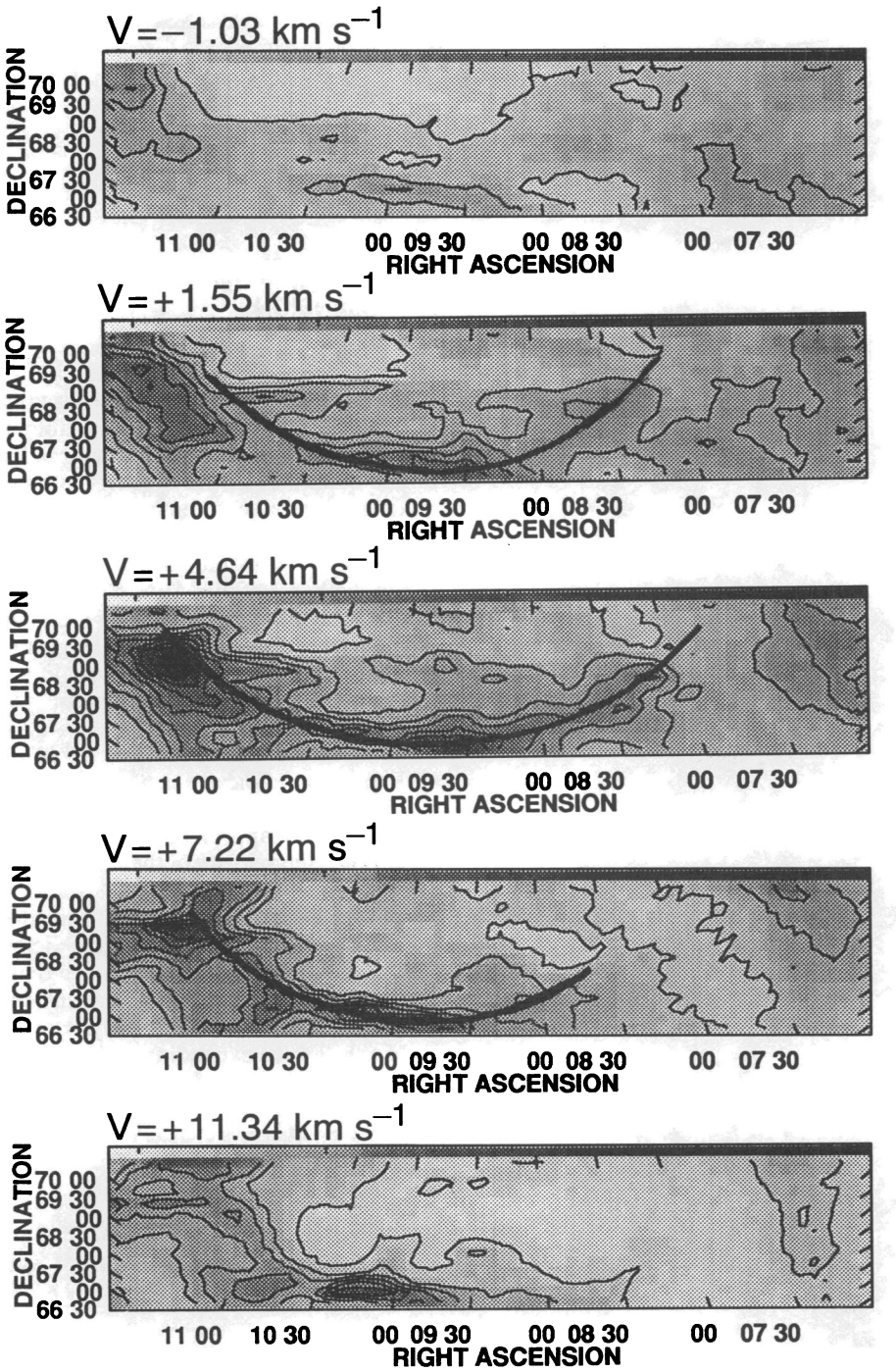

FIG. 6a

FIG. 6.—H I velocity channel maps for (*a*) MBM 27–29 and (*b*) and (*c*) MBM 53–55. Each panel covers a velocity interval $\Delta V = 0.52$ km s^{-1} with its central velocity marked on the top. The heavy curve represents the ridge line of the H I. The dashed curve on the MBM 53–55 maps represents the other arclike feature which shows no apparent expansion.

authors conclude that the enhancement is likely the result of hot gas produced by stellar winds which have evacuated the cavity and created the shell. The shell is clearly noticeable in both global representations of *IRAS* 100 μm data and low-resolution H I low-velocity data. Since MBM 18 and MBM 20 are embedded in parts of the shell, it is likely that these objects share a common origin.

4. DISCUSSION

4.1. *The Association of HLCs and* H I *Gas*

A large fraction of the local H I gas, as shown in Figure 1, is distributed in filamentary or looplike structures. These H I filaments, in general, cover an area of hundreds of square degrees with the HLCs invariably projected within the bound-

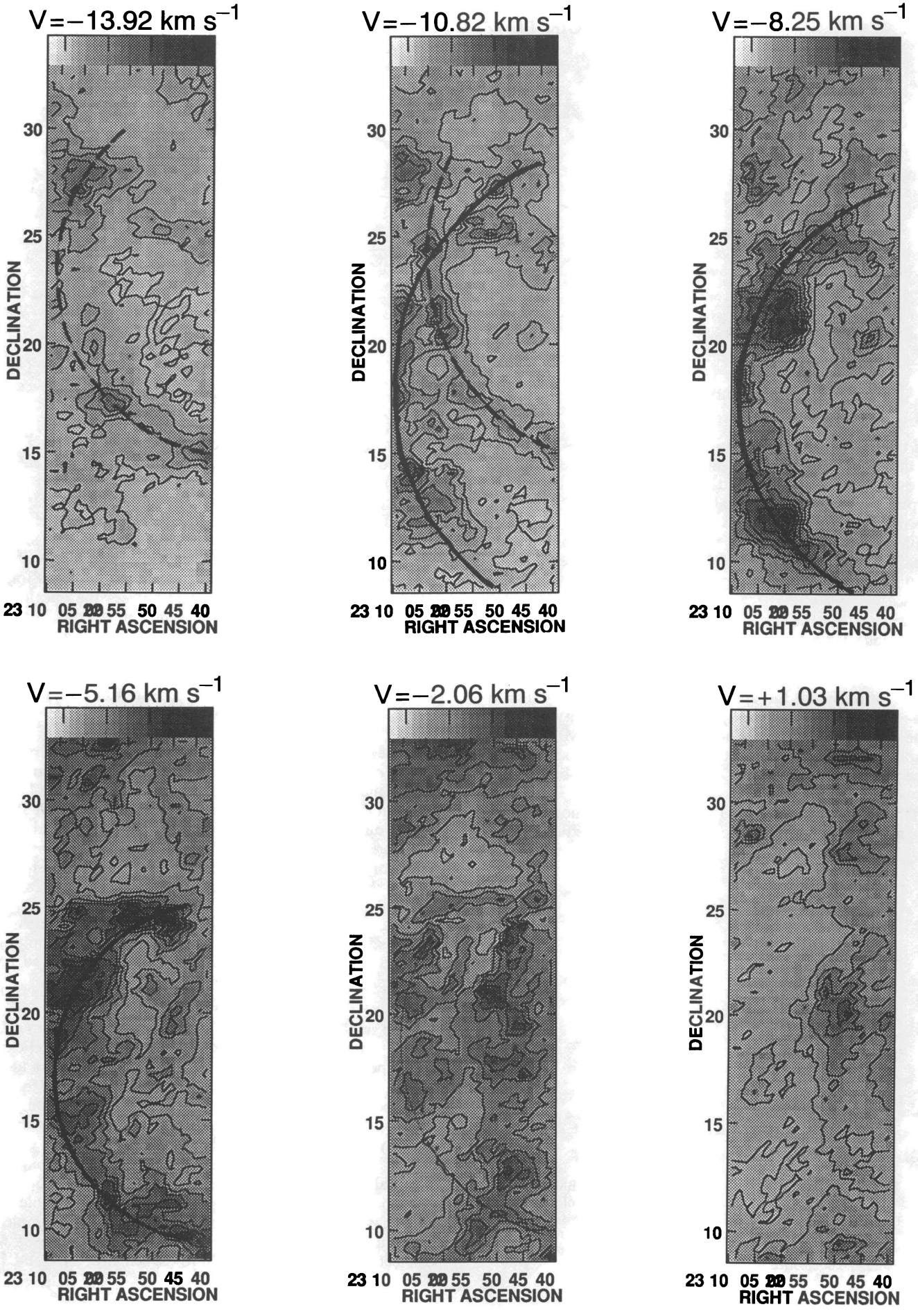

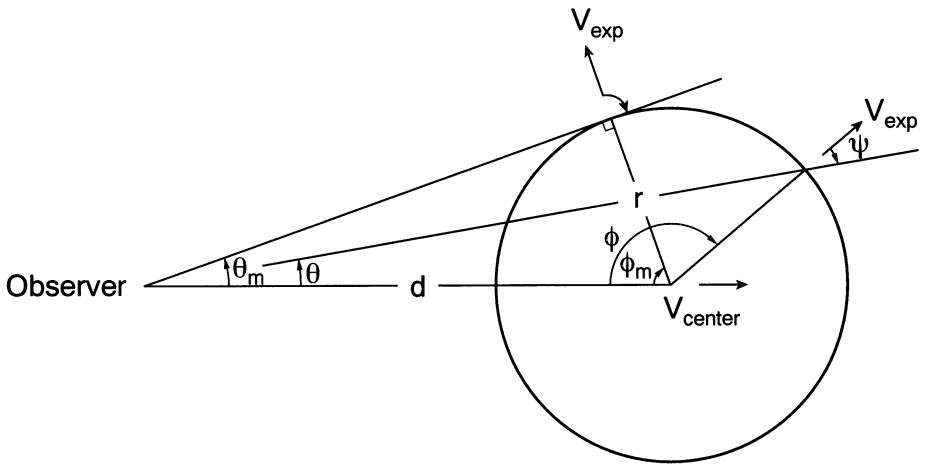

FIG. 7.—Diagram for derivation of the expansion velocity of an expanding shell (see § 3.4). Note that in our case r is comparable to d.

aries of the H I structures. Moreover, from Figure 2, we find that there is always a component of the H I associated with the CO, even though in some clouds there are multiple blended H I components. The close association of the HLCs with the H I, both in projected area and in velocity, implies that the HLCs are physically associated with some of the H I gas on a global scale. Since typical distances of the HLCs are of order 100–300 pc (Blitz 1991), the corresponding H I features are at the same distance.

In general, the H I spectrum of the 18 clouds in our sample can be collected into a few distinct groups according to the complexity of their line shapes. For MBM 20 and MBM 40, the spectra show a single isolated H I peak at the CO velocity. On the other hand, the spectra of MBM 27–29 and MBM 41–44 show an H I peak with extended low-intensity emission at the cloud's CO velocity. For MBM 23–24, MBM 25, MBM 49, and MBM 53–55, the spectra show multiple peaks with one of the peaks centered on the CO velocity and with other emission components overlapped to some degree. The spectra of the remaining clouds, MBM 16 and MBM 18, show complicated profiles with the components blended together. This is

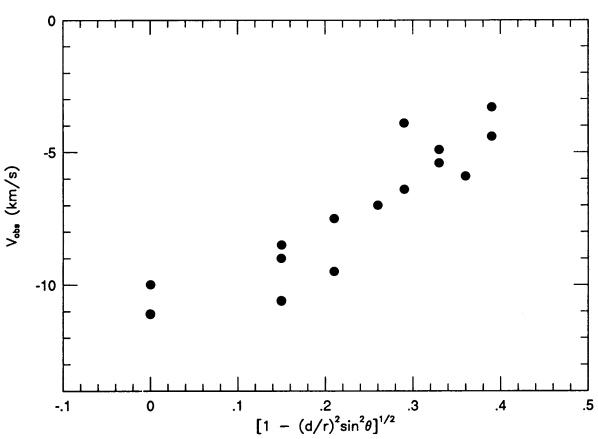

FIG. 8.—The observed velocity of the shell in which MBM 53–55 are embedded for various velocity channels plotted as a function of the quantity $[1-(d/r)^2\sin^2\theta]^{1/2}$. The right-hand term is equivalent to $\cos\psi$ in Fig. 7, where ψ is the angle between the line of sight of the observer and the radial expansion velocity vector. One of the data points gives an imaginary value for the ordinate and is not plotted.

not surprising since these two clouds are embedded in a large region of 100 μm emission extending south (in Galactic latitude) of the Taurus-Auriga dark clouds. Magnani (1988) has speculated that this region may be a more diffuse extension of the Taurus-Auriga dark cloud complex. Since the entire region is rich in gas and dust, the H I line intensities are strongest here (see Fig. 3) and the H I component associated with the HLCs is hidden in the foreground and background emission.

The association of the CO and H I raises the question of whether the HLCs were created in situ or whether they are preexisting and have been entrained by the passing H I shells. We note that the velocity dispersion of the HLCs is 5.4 km s^{-1} (MBM). If the velocity dispersion of the filaments has a similar value (values of 3–7 km s^{-1} have appeared in the literature), then the likelihood of seeing the close correspondence between the CO and H I velocities for such a large number of clouds would be very small. Moreover, we would expect that most of the CO detected to date would be outside the shells and filaments if their volume filling fraction is as small as the 20% that has been inferred (Van Buren 1989). Elmegreen (1988) has pointed out that groups of HLCs share similar internal velocity dispersions and LSR velocities. These considerations imply that a common formation mechanism may be responsible for creating the various groups of clouds. Since the groups appear to be embedded in large H I structures, the most likely conclusion is that the clouds formed in situ in the H I loops and filaments. A group of entrained, preexisting clouds would not necessarily show similar internal velocity dispersion and LSR velocities.

4.2. *The Offsets between* CO *and* H I

In the small-scale analysis of the H I and CO data, an offset generally comparable to the cloud linear size of the CO cloud was found in all of the clouds between the CO peak and the nearest H I peak. However, no systematic pattern for the offsets between the CO and H I has been found from our data sample, either with respect to the Galactic plane or from an arbitrary center of expansion. The lack of any obvious pattern suggests that the CO–H I offset is probably not determined by large-scale processes but is determined by local conditions.

One possible explanation for the offsets is that the molecular clouds have condensed out of the atomic gas. As an example, in a uniform, spherical H I cloud, the highest column density will be detected along the line of sight to the center of the cloud. If a

phase transition from atomic to moleculr gas occurs near the center of the cloud, some of the H I would be converted to H_2 and the H I peak would consequently be shifted from the peak of the CO emission. The separation of the offset from the center of the H I peak depends on the size of the region that undergoes the phase transition, but should in any case be comparable to the size of the CO cloud. Table 3 clearly shows that for most clouds the CO–H I offset is comparable to the effective diameter of the molecular clouds. The similarity of this size scale from cloud to cloud is consistent with the idea that the offsets are due to a phase transition.

4.3. H I *Envelopes around HLCs*

An association between atomic and molecular hydrogen in interstelar clouds is known to exist both from theoretical considerations and from observations. On a large scale, several Galactic surveys show that molecular clouds contain residual H I (e.g., Burton, Liszt, & Baker 1978; Baker & Burton 1979; Liszt, Burton, & Bania 1981). On small scales, H I observations demonstrate that the atomic gas is clearly related to the molecular component in many sources (see Blitz 1987; Elmegreen & Elmegreen 1987 for references) including nearby dark clouds, where H I self-absorption has been observed (Knapp 1974 and references therein). While most of these studies describe the association of the atomic and molecular gas, detailed analyses of the H I–H_2 morphology are less common. Mattila & Sandell (1979) and Liljeström & Mattila (1988) observed the 21 cm line in a number of dark nebulae and suggested that an H I layer surrounds the inner molecular region. A similar conclusion was reached by Wannier, Lichten, & Morris (1983) in a study of five giant molecular clouds, by Grabelsky et al. (1987) for CO clouds in the outer Galaxy, by Elmegreen & Elmegreen (1987) for giant molecular clouds in the inner Galaxy, and by Wannier et al. (1991) for 14 molecular clouds of various types.

From a theoretical standpoint, the formation of H_2 is assisted by the shielding of line radiation by the H_2 that has already formed (self-shielding) and by the presence of dust within an H I layer that provides the nucleation sites for the H_2 molecules. After a critical column density of H I is reached, the H_2 self-shields, with the outer layer absorbing the dissociating Lyman lines, and any additional hydrogen inside this layer becomes molecular (Hollenbach, Werner, & Saltpeter 1971; Federman, Glassgold, & Kwan 1979). The critical density of H I depends only on the ratio G/n, where G is the integral over frequency of the ambient interstellar flux times the cross section in the H_2 Lyman band, and n is the volume density of hydrogen atoms. Shaya & Federman (1987) express this relationship in terms of a critical radius, R_{cr}, for the H I–H_2 transition beyond which clouds become molecular. This relationship can be expressed as $R_{cr} \propto G^{1.4} n^{-2.4}$. Since the radius depends on the radiation field, the H I layer around molecular clouds will be smaller as the radiation field diminishes.

Empirically, studies of diffuse clouds have shown that the column density of H_2 rises precipitously for visual extinctions >0.25 mag (Savage et al. 1977; Blitz, Bazell, & Désert 1990). For interstellar clouds on the borderline between diffuse and translucent clouds (defined to be $A_v \sim 1$ mag; see van Dishoeck & Black 1988), the H I and H_2 column densities are found to be comparable to one another. This result was established in a preliminary fashion for the HLCs by Blitz et al. (1984) from an observational standpoint, and by van Dishoeck & Black (1986) from a theoretical standpoint.

TABLE 6

RATIOS OF THE H I TO CO LINEWIDTHS AND COLUMN DENSITIES

Clouds (MBM)	$\frac{\sigma(\text{H I})}{\sigma(\text{CO})}$	$0.33\left[\frac{\sigma(\text{H I})}{\sigma(\text{CO})}\right]^{4/3}$	$\frac{\langle N(H_2)\rangle}{N(\text{H I})_{peak}}$	$\frac{2\langle N(H_2)\rangle}{\langle N(H_{total})\rangle}$
16	6.4	3.9	0.4	0.51
18	4.5	2.5	1.1	0.75
20	2.8	1.3	2.0	0.88
23	6.3	3.8	0.7	0.63
24	4.1	2.2	0.8	0.65
25	7.5	4.8	1.3	0.75
27	2.8	1.3	4.4	0.93
28	4.0	2.1	4.2	0.92
29	2.0	0.8	3.9	0.92
40	10.0	7.1	0.5	0.55
41	6.3	3.8	4.6	0.94
42	10.0	7.1	3.7	0.92
43	10.0	7.1	3.8	0.93
44	8.3	5.5	3.2	0.90
49	2.7	1.2	1.2	0.72
53	5.8	3.4	4.7	0.93
54	4.8	2.7	5.7	0.94
55	4.9	2.7	5.0	0.92
Mean	5.7	3.5	2.8	0.82
Uncertainty	0.6	0.5	0.4	0.03

The mean fractional abundance of the H_2 over the cloud area, $\langle 2N(H_2)\rangle/\langle N(H_{total})\rangle$, is listed in the last column of Table 6 with a mean value of 0.82, and varies from 0.51 to 0.94. This value is slightly greater than the fractional abundance of H_2 reported for typical diffuse interstellar clouds with $A_v \sim 1$ mag such as o Per, ζ Per, ζ Oph [$(2N(H_2)/N(\text{H I}) \sim 0.6$; van Dishoeck & Black 1986]. The HLCs have visual extinctions averaged over areas on the scale of H I sampling (10′–20′) of ~ 1 mag (Mafnani & de Vries 1986) and are for the most part, translucent clouds. Models of translucent molecular clouds (van Dishoeck & Black 1988) have higher values of $N(H_2)$ than the diffuse cloud models and consequently the ratios of $N(H_2)/N(H_{total})$ for a large set of cloud models are consistent with our observations.

Our data reveal that in HLCs there exists a "threshold" for the wholesale conversion of hydrogen nucleons to the molecular phase at a $N(H_{total})$ of $\sim 5 \times 10^{20}$ cm^{-2}. This is most easily seen in Figure 9 which shows that a column densities greater

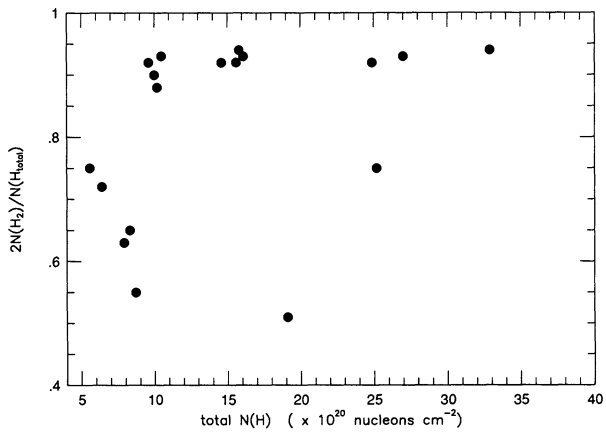

FIG. 9.—The fraction of protons in molecular form plotted as a function of the total number of hydrogen nucleons. At a threshold of $N(H_{total}) > 5 \times 10^{20}$ cm^{-2}, most of the hydrogen nucleons are in the form of H_2.

than 5×10^{20} cm^{-2} most of the hydrogen nucleons are in molecular form. This threshold is consistent with the theoretical arguments outlined above; the exact value of the threshold probably results from the intensity of the local UV radiation field. We note that the mean fractional abundance of H_2 along the line of sight is never less than 0.5. If the clouds are, on average, as young as the 2×10^6 yr estimated by MBM, then some of the clouds should be considerably younger than the mean. The lower limit to the fractional abundance suggests that either there is a rapid conversion from H I to H_2 once a cloud becomes molecular, or more probably that the CO abundance increases rapidly once the cloud is sufficiently opaque (i.e., $A_V \geq 0.25$ mag). Recall that the H_2 column density is inferred from the CO line strength so the only direct information available to us in this analysis is from the CO data. Blitz et al. (1990) showed that the CO observations of the clouds identified by Désert, Bazell, & Boulanger (1988) can be best understood if the clouds with visual extinctions less than 0.25 mag have CO abundances similar to those in diffuse clouds ($\sim 10^{-6}$), and those with higher extinction have abundances like those in translucent or dark clouds ($\sim 10^{-5}$ to 10^{-4}). If the clouds are randomly distributed in age, an estimate of the conversion time can be made from the estimated mean age of 2×10^6 yr divided by the number of clouds likely to be younger than this; i.e., half the sample, or nine clouds. Thus an estimate of the upper limit for the timescale of generating a typical transluscent cloud CO abundance is $\sim 2 \times 10^5$ yr.

It is worth noting that the numerical results quoted in this paper are based on the CO to H_2 conversion ratio stated in § 3.3. Some workers suggest that this conversion ratio for at least some HLCs is lower than the one we used. The immediate consequence of lowering the conversion ratio is to lower the values of $N(H_2)$ in direct proportion to the conversion ratio. A lower value would not change the conclusions of this paper, nor would it even alter the threshold value of 5×10^{20} cm^{-2} very much since the total column densities of most clouds near the threshold are dominated by H I. In any event, we do not believe that such a large downward revision is warranted because the studies that suggest a lower CO/H_2 conversion (de Vries et al. 1987; Heithausen & Mebold 1989) are based on only a few clouds and on the questionable assumptions mentioned in § 3.3. On the other hand, Magnani et al. (1988) showed a large variation in the $N(H_2)/I(CO)$ factor which can encompass the low values found by de Vries et al. (1988) and Heithausen & Mebold (1989). Furthermore, the higher value is supported by the observations of de Vries & van Dishoeck (1988) and Magnani & Onello (1993).

4.4. *The Condensation of Molecular Clouds*

The observations presented to this point suggest that the CO clouds have formed from the H I swept up in shells and filaments. Moreover, there appears to be a minimum H I column density needed to form molecular clouds detectable in the radio lines of CO, and that the fractional abundance of CO appears to be related to the column of CO swept up in the shells and filaments. The question thus arises, what is the physical mechanism that drives the molecule formation? Can we unambiguously predict where molecules will form in the interstellar medium?

The most obvious mechanism is that of a thermal instability arising from the opacity of the H I column due to shielding of the continuum by the dust and the self shielding of the line radiation by the column of H_2 that builds up along the line of sight, as discussed in § 4.1. In this case, we expect that

$$\frac{n(H_2)}{n(\mathrm{H\ I})} \simeq \frac{1}{2}\left[\frac{\Delta V(\mathrm{H\ I})}{\Delta V(\mathrm{CO})}\right]^2 = \frac{1}{2}\left[\frac{\sigma(\mathrm{H\ I})}{\sigma(\mathrm{CO})}\right]^2, \quad (4)$$

where n is the volume density, ΔV is the full width at half-maximum of the H I or CO line, and σ is the velocity dispersion of the gas, in this case due to thermal Doppler broading. If the gas undergoes a change of phase, and there is a simple isotropic compression of the molecular gas under conditions of pressure equilibrium because of the lower temperature of the molecular gas, then we find that

$$\frac{\langle N(H_2)\rangle}{N(\mathrm{H\ I})_{\mathrm{peak}}} = 0.53\left[\frac{n(H_2)}{n(\mathrm{H\ I})}\right]^{2/3} \simeq 0.33\left[\frac{\sigma(\mathrm{H\ I})}{\sigma(\mathrm{CO})}\right]^{4/3}. \quad (5)$$

Here, $\langle N(H_2)\rangle$ is the mean H_2 density along the line of sight (to account for clumpiness), and $N(\mathrm{H\ I})_{\mathrm{peak}}$ is the maximum column density of the *uncondensed* H I.

Linewidths for the CO ($J = 1$–0) transition with velocity widths less than 0.4 km s^{-1} are only rarely seen in molecular clouds. Typical CO linewidths imply kinetic temperatures of >500 K for CO in thermal equilibrium with H_2. For the clouds we have observed, the excitation temperatures are never more than 15 K, and typically they are lower. In addition, the associated dust temperatures determined from *IRAS* observations are invariably 20–25 K (e.g., Weiland et al. 1986). Since the CO molecule is almost always optically thick in Galactic molecular clouds, its excitation temperature should be close to the kinetic temperature. The discrepancy between the two estimates suggests that the CO lines are not thermally broadened but that the widths are due to bulk motion of the gas, and that σ is a measure of this motion. There is reasonable evidence from what is known about the magnetic fields that the bulk motions are the result of magnetosonic turbulence, but the velocity dispersions are less than or equal to the Alfvén velocity in the gas (Blitz 1993). It is therefore likely that the gas motions are sub-Alfvénic and that the motions may be quite long lived compared to hydrodynamic supersonic turbulence. In this case, σ is due to the bulk motions rather than thermal broadening.

On the other hand, equation (4) results from the *assumption* of pressure equilibrium, and it is unclear how a thermal instability is manifested under the conditions of magnetosonic turbulence. Furthermore, several additional factors complicate the observational picture. The column densities derived here assume a single ratio to convert the observed CO transition to $N(H_2)$. CO abundances are known to vary by large factors for clouds in the range of extinction manifested by the high latitude clouds (see § 4.3), and thus the molecular densities may not be very well determined from the CO $J = 1$–0 transition alone. Furthermore variations in the ambient ultraviolet radiation field can produce large CO abundance variations (e.g., Gredel et al. 1992). Our observations produce only approximate line-of-sight column densities, but the relevant column density is the minimum column exposed to the ambient radiation field. For the shell-like and filamentary geometries prevalent here, the minimum column may be significantly different from what we measure.

We have nevertheless attempted to evaluate whether equation (5) is supported by the data and have found the results to be inconclusive. Without independent information on the gas densities (from multitransition observations, for example), it

becomes difficult to evaluate n, and the geometric complications suggest that it is difficult to evaluate equation (5) even if it were valid under the conditions of magnetosonic turbulence. We are therefore unable to pinpoint a precise mechanism for the molecular condensation process, even though the evidence that the molecular clouds have formed from the H I appears to be quite good.

4.5. CO *and* H I *Linewidths and Energy Considerations*

If the HLCs formed within the H I shells and structures described above, the CO and H I linewidths might be expected to be correlated with one another. Figure 10*a* is a plot of the velocity dispersions of the CO emission lines and the H I components associated with the various clouds. A weak correlation is present in the data; the correlation coefficient is 0.41 suggesting that there is a 10% probability that the data are uncorrelated. However, the correlation is sufficiently weak that no conclusions can be drawn from the values of the velocity dispersions.

In an analysis of the H I associated with a number of giant, self-gravitating clouds, Andersson, Wannier, & Morris (1991) also found no clear trend between H I and CO linewidths at the edges of the clouds. We note, however, that the mean ratio of the H I CO linewidths is 5.7 in our sample and 8.1 in the Andersson sample (taken from their Fig. 7*b*), suggesting that the ratios of the linewidths are not too dissimilar for self-gravitating and non–self-gravitating clouds.

In Figure 10*b* we plot $\sigma_{\rm int}$ versus σ(H I). Recall that $\sigma_{\rm int}$ represents the velocity dispersion among the clumps in a CO cloud and is used by MBM to determine the overall kinetic energy of an HLC. If a particular HLC has condensed from the surrounding H I, there may also be a correlation between these two quantities. However, both the figure and a statistical analysis suggest that the two velocity dispersions are uncorrelated. If we use the data in Table 2 to calculate how the mean kinetic energy per particle is distributed between the two atomic and molecular gas phases, we find that the ratio $m_{\rm H\,I}\sigma^2$(H I)/$m_{\rm CO}\sigma^2$(CO) varies by a factor of 25 from cloud to cloud. Despite this range, the mean ratio of this quantity for the ensemble of clouds is 1.2. *Although there is considerable variation from cloud to cloud, our results suggest that, on average, there is energy equipartion between the atomic and molecular phases of the gas.* We find no obvious relationship between the size of this ratio and the morphology of either the CO or the H I. However, we do note that MBM 41–44, the molecular clouds associated with the Draco Nebula, have the highest value of this ratio. It has been suggested that the Draco Nebula is the result of gas from the halo raining down onto the disk (Goerigk & Mebold 1986; Odenwald 1988), and thus its origin and formation mechanism is likely to be different from the other HLCs.

4.6. *Individual Cloud Complexes*

4.6.1. *MBM 20*

The Lynds dark cloud 1642, which comprises MBM 20, has been known for a decade to be associated with H I emission (Taylor, Taylor, & Vaile 1982). Later studies in the far-infrared and optical regions revealed that the cloud is located in the head of a cometary H I nebula (Laureijs, Mattila, & Schnur 1987; Liljeström & Mattila 1988). Sandell, Reipurth, & Gahm (1987) confirmed that two infrared point sources are a pair of T Tauri stars embedded in the cloud core.

MBM 20 is one of the only two HLCs in the MBM catalog which is a known site of star formation (the other is MBM 12; Magnani, Caillault, & Armus 1990). Liljeström (1991) calculated $\sigma_{\rm vir}$ by assuming a homogeneous and spherical cloud at a distance of 100 pc and argued that MBM 20 is in virial equilibrium, a conclusion which is not surprising in view of the observed star formation.

Because MBM 20 is a dark cloud in which star formation is observed, it probably represents the most advanced state of evolution of any of the HLCs. However, the cloud is not unusual in terms of either its total column density, its average H I or H_2 column density, or the ratio between the two. It is remarkable however, for the narrowness of the H I and H_2 lines, and for the narrowness of the H I line relative to the CO line (see Table 6). Unlike most HLCs, gravity is important in the dynamics and line profiles of MBM 20. Moreover, the location of the cloud in the loop-like structure surrounding the Eridanus soft X-ray enhancement (Burrows et al. 1993) indicates that a dark cloud may be able to form in the same way as we describe for the translucent clouds.

4.6.2. *MBM 27–29*

The clouds which comprise the MBM 27–29 complex are typical high-latitude clouds, lying along a large fraction of an

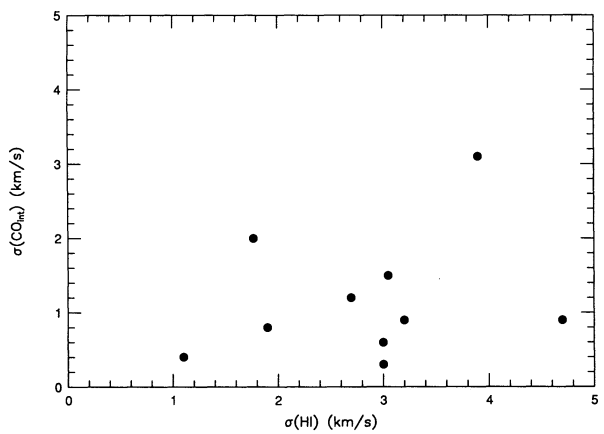

FIG. 10*a*

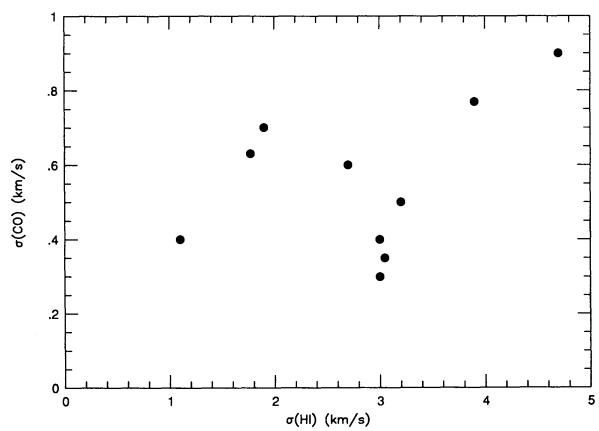

FIG. 10*b*

FIG. 10.—(*a*) The velocity dispersion of the CO (J = 1–0) line as a function of the H I velocity dispersion. The plotted quantities are obtained from Table 2 but are averaged over the objects comprising a "cloud complex" (see MBM). (*b*) Same as (*a*) but the CO dispersion represents the variance in CO Gaussian-fit centroid velocities (see § 4.5).

H I arc. In Figure 3*f*, a clear H I line component at the V_{LSR} of this complex is apparent. Figure 4*f* shows a shell-like structure in the observed area, suggesting that the formation of the MBM 27–29 complex is related to the evolution of the H I shell. The high H_2 fractional abundance values for this complex indicate that the phase transition from atomic to molecular is quite complete if the clouds had been formed from H I. Although the velocity structure of the H I shell is too ambiguous to be identified as expanding from our data, an interstellar shock or stellar wind is still a possible mechanism for the formation of the shell and the subsequent condensation of the CO clouds. Such a mechanism has been suggested by Meyerdierks et al. (1991).

4.6.3. *MBM 41–44*

The complex of clouds MBM 41–44 are intermediate velocity objects and have been extensively studied by Mebold et al. (1985). These clouds appear to be prototypes of a class of relatively high velocity local molecular clouds discussed by Blitz (1991). They all have large negative velocities; the LSR velocity ranges from -20 km s^{-1} to -25 km s^{-1}, four standard deviations from the V_{LSR} of typical HLCs, much higher than the velocity dispersion of the ensemble of HLCs. Goerigk & Mebold (1986) suggest that the MBM 41–44 complex, which they call the Draco Cloud, is at a distance >800 pc and is therefore at the disk-halo interface of the Galaxy. This large distance is, however, controversial (Blitz 1991). This cloud complex, like two others discussed by Blitz (1991), has a cometary morphology and both Goerigk & Mebold (1986) and Odenwald (1988) suggest that it is an example of a cloud that may be "raining" onto the disk of the Galaxy from the halo. If so, the formation of the molecular cloud may have taken place somewhere other than in a local shell or filament and the mechanism responsible for the formation of the cloud may be quite different than the one proposed in this paper for the other HLCs.

4.6.4. *MBM 53–55*

From the data presented in § 3.4, we find that the MBM 53–55 H I shell is expanding with a velocity of 18 km s^{-1}. This complex, which, incidentally has the largest projected area on the sky of any of the MBM clouds, is the clearest example of molecular clouds formed by shock compression in an expanding shell. These clouds also have the highest value of $\langle N(H_2)\rangle/N(\text{H I})_{peak}$ of any of the clouds in our sample, suggesting the most complete conversion of H I to H_2. A likely candidate for providing the mechanical energy necessary to create an expanding shell is a supernova remnant (SNR). This mechanism has already been invoked for creating the Eridanus shell (Heiles 1976), a structure similar to the MBM 53–55 shell. The energy necessary to create the Eridanus shell, 3.8×10^{50} ergs, calls for a supernova possibly energizing a pre-ionized cavity.

The kinetic energy of the MBM 53–55 expanding shell can be obtained by adding the kinetic energy of each portion (projected arc of a given channel map) together, i.e., K.E. = $\frac{1}{2}V_{exp}^2 \sum M$, where M is the mass of one of the arcs in our channel maps. Assuming a distance of 200 pc (the estimated median distance of this cloud complex; Welty et al. 1989), the mass for the H I shell is about $3 \times 10^3\ M_\odot$, and the kinetic energy, 1×10^{49} ergs. Including the H_2 inferred from the CO observations increases this energy by a factor of about 4 to 4×10^{49} ergs.

If only 1% of the energy of the supernova explosion goes into the kinetic energy of shell, as we currently believe (Woltjer 1972), the outburst energy necessary for the creation of MBM 53–55 is about 4×10^{51} ergs. This suggests that MBM 53–55 could have been formed by a few supernovae or another similarly large mechanical input of energy such as the stellar wind from an association of early O stars. Because the other shells presumably exhibit small expansion velocities, even less energy is needed to explain the morphology of the typical HLC H I shell or filament. Therefore, events less energetic than supernovae, might explain some of the shells and filaments seen in the figures.

5. CONCLUSIONS

The main conclusions of this paper can be summarized as follows:

1. In a large-scale comparison, all 75 HLCs in our data sample are found to be associated with H I gas both in position and velocity with most of the HLCs lying along filamentary or loop-like H I structures. This conclusion is supported by a Gaussian deconvolution of the H I spectra in which it is found that there is always one strong H I component essentially coincident with the CO velocity.
2. In a small-scale comparison, we found from the contour maps that the CO and H I emission peaks are typically offset from one another by about the same linear size as the HLCs, about 1°.5. No obvious symmetric pattern of these CO–H I offsets was found with respect to either the Galactic plane or toward an arbitrary explosion center. This suggests that the offset results from physical conditions local to the molecular clouds.
3. We find that there is a minimum total column density of 5×10^{20} cm^{-2} observed along any line of sight in which CO clouds are found. The fractional abundance of H_2 nucleons is never found to be less than 0.5 in any of the clouds for our assumed CO/H_2 coversion ratio.
4. The good agreement between the H I and CO radial velocities and the morphological association between the CO and H I peaks suggests that the molecular clouds were formed in situ and were not preexisting clouds entrained by expanding H I shells and filaments.
5. No apparent correlation of the CO and the H I linewidths is found. There is, however, a rough equipartition of the kinetic energy between the H I and the CO gas although there is considerable variation from cloud to cloud.
6. Two of the 10 observed H I regions, which are associated with the MBM 27–29 and MBM 53–55, respectively, show clear arclike structures. In addition, two more HLCs are embedded in a looplike structure attributed by Burrows et al. to a wind-blown bubble. The MBM 53–55 shell is found to be expanding. An expansion velocity for the latter shell of about 18 km s^{-1} is obtained, and the kinetic energy of the expanding shell is estimated to be 4×10^{49} ergs. The shell could have been formed by a supernova explosion or stellar winds, and so shocks may be responsible for at least some of the conversion of H I to H_2.

The authors thank C. Heiles for providing the H I photos, F. J. Lockman for help with the observations and with the reduction of the 43 m H I data, R. Maddalena and M. Pound for observing some of the H I and CO lines of sight which provided the information on the linewidths, and K. Ferrier for a helpful discussion of the role of the magnetic field in H I shells. This work is supported by the NSF grant AST 89-18912.

REFERENCES

Andersson, B. G, Wannier, P. G., & Morris, M. 1991, ApJ, 366, 464
Baker, P. L., & Burton, W. B. 1979, A&AS, 35, 129
Blitz, L. 1987, in The Evolution of Galaxies, ed. J. Palous (Prague: Czechoslovak Academy of Science), 201
———. 1991, in Molecular Clouds, ed. R. A. James & T. J. Millar (Cambridge: Cambridge Univ. Press), 49
Blitz, L. 1993, in Protostars and Planets III, ed. E. Levy & J. Lunine (Tucson: Univ. of Arizona Press), 125
Blitz, L., Bazell, D., & Désert, F. X. 1990, ApJ, 352, L13
Blitz, L., Magnani, L., & Mundy, L. 1984, ApJ, 282, L9
Bloemen, J. B. G. M. 1987, ApJ, 322, 694
Bloemen, J. B. G. M., et al. 1986, A&A, 154, 25
Boulanger, F., & Pérault, M. 1988, ApJ, 330, 964
Burrows, D. N., Singh, K. P., Nousek, J. A., Garmire, J. P., & Good, J. 1993, ApJ, 406, 97
Burton, W. B., Liszt, H. S., & Baker, P. L. 1978, ApJ, 219, L67
Cappa de Nicolau, C. E., & Pöppel, W. G. L. 1986, A&A, 164, 274
Colomb, F. R., Pöppel, W. G. L., & Heiles, C. 1980, A&AS, 40, 47 (CPH)
de Geus, E. 1988, Ph.D. thesis, Leiden Univ.
Désert, F. X., Bazell, D., & Boulanger, F. 1988, ApJ, 334, 815
de Vries, H. W., Heithausen, A., & Thaddeus, P. 1987, ApJ, 319, 723
de Vries, C. P., & van Dishoeck, E. F. 1988, A&A, 203, L23
Dickman, R. L., & Kleiner, S. C. 1985, ApJ, 295, 479
Elmegreen, B. G. 1988, ApJ, 326, 616
Elmegreen, B. G., & Elmegreen, D. M. 1987, ApJ, 320, 182
Federman, S. R., Glassgold, A. E., & Kwan, J. 1979, ApJ, 227, 466
Goerigk, W., & Mebold, U. 1986, A&A, 162, 279
Grabelsky, D. A., Cohen, R. S., Bronfan, L., Thaddeus, P., & May, J. 1987, ApJ, 315, 122
Gredel, R., van Dishoeck, E. F., de Vries, C. P., & Black, J. H. 1992, A&A, 257, 245
Heiles, C. 1976, ApJ, 208, L137
———. 1979, ApJ, 229, 533
———. 1984, ApJ, 55, 585
Heiles, C., & Habing, H. J. 1974, A&AS, 14, 1
Heithausen, A., & Mebold, U. 1989, A&A, 214, 347
Hollenbach, D. J., Werner, M. W., & Salpeter, E. E. 1971, ApJ, 163, 165
Keto, E. R., & Myers, P. C. 1986, ApJ, 304, 466 (KM)
Knapp, S. L. 1974, Ph.D. thesis, Univ. of Maryland
Kulkarni, S., & Heiles, C. 1987, in Interstellar Processes, ed. D. J. Hollenbach & H. A. Thronson Jr. (Dordrecht: Reidel), 87
Laureijs, R. J., Mattila, K., & Schnur, G. 1987, A&A, 184, 269
Liszt, H. S., Burton, W. B., & Bania, T. M. 1981, ApJ, 246, 74
Liljeström, T. 1991, A&A, 244, 483
Liljeström, T., & Mattila, K. 1988, A&A, 196, 243
Lockman, F. J., Jahoda, K., & McCammon, D. 1986, ApJ, 302, 432
Lynds, B. T. 1962, ApJS, 7, 1
Magnani, L. 1987, Ph.D. thesis, Univ. of Maryland
———. 1988, in The Outer Galaxy, ed. L. Blitz & F. J. Lockman (New York: Springer-Verlag), 168
Magnani, L., Blitz, L., & Mundy, L. 1985, ApJ, 295, 402 (MBM)
Magnani, L., Blitz, L., & Wouterloot, J. G. A. 1988, ApJ, 326, 909
Magnani, L., Caillault, J-P., & Armus, L. 1990, ApJ, 357, 602
Magnani, L., & de Vries, L. P. 1986, A&A, 168, 271
Magnani, L., & Onello, J. S. 1993, ApJ, 408, 559
Mattila, K., & Sandell, G. 1979, A&A, 78, 264
Mebold, U., Cernicharo, J., Velden, L., Reif, K., Crezelius, C., & Goerigk, W. 1985, A&A, 151, 427
Mebold, U., Heithausen, A., & de Vries, H. W. 1988, in Molecular Clouds in the Milky Way and External Galaxies, ed. R. L. Dickman, R. L. Snell, & J. S. Young (Berlin: Springer-Verlag), 101
Meyerdierks, H., Heithausen, A., & Reif, K. 1991, A&A, 245, 247
Odenwald, S. F. 1988, ApJ, 325, 320
Sandell, G., Reipurth, R., & Gahm, G. F. 1987, A&A, 181, 283
Savage, B. D., Bohlin, R. C., Drake, J. F., & Budich, W. 1977, ApJ, 216, 291
Shaya, E. J., & Federman, S. R. 1987, ApJ, 319, 76
Spitzer, L. 1978, Physical Processes in the Interstellar Medium (New York: John Wiley & Sons)
Taylor, M. I., Taylor, K. N. R., & Vaile, R. A. 1982, Proc. Astron. Soc. Australia, 4, 440
Turner, B. T., Xu, L.-P, & Rickard, L. J. 1992, ApJ, 391, 158
Van Buren, D. 1989, ApJ, 338, 147
van Dishoeck, E. F., & Black, J. H. 1986, ApJS, 62, 109
———. 1988, ApJ, 334, 711
Verschuur, G. L., & Magnani, L. 1994, AJ, 107, 287
Verschuur, G. L., & Schmelz, J. T. 1989, AJ, 98, 267
Wannier, P. G., Andersson, B-G, Morris, M., & Lichten, S. M. 1991, ApJS, 75, 987
Wannier, P. G., Lichten, S. M., & Morris, M. 1983, ApJ, 268, 727
Weiland, J., Blitz, L., Dwek, E., Hauser, M. G., Magnani, L., & Rickard, L. J. 1986, ApJ, 306, 463
Welty, D. E., Hobbs, L. M., Blitz, L., & Penprase, B. E. 1989, ApJ, 346, 232
Woltjer, L. 1972, ARA&A, 10, 129